Search for an LSP gluino at LEP with the DELPHI detector

J. Abdallah, P. Abreu, W. Adam, P. Adzic, T. Albrecht, T. Alderweireld, R. Alemany-Fernandez, T. Allmendinger, P P. Allport, U. Amaldi, et al.

EUROPEAN ORGANIZATION FOR NUCLEAR RESEARCH

CERN–EP/2002-076

8 August 2002

Search for an LSP gluino at LEP with the DELPHI detector

DELPHI Collaboration

Abstract

In some supersymmetric models, the gluino ($\widetilde{\mathrm{g}}$) is predicted to be light and stable. In that case, it would hadronize to form R-hadrons. In these models, the missing energy signature of the lightest supersymmetric particle is no longer valid, even if R-parity is conserved. Therefore, such a gluino is not constrained by hadron collider results, which looked for the decay $\widetilde{\mathrm{g}} \rightarrow \mathrm{q\bar{q}}\widetilde{\chi}_1^0$.
Data collected by the DELPHI detector in 1994 at 91.2 GeV have been analysed to search for $\mathrm{q\bar{q}}\widetilde{\mathrm{g}}\widetilde{\mathrm{g}}$ events. No deviation from Standard Model predictions is observed and a gluino mass between 2 and 18 GeV/c^2 is excluded at the 95% confidence level in these models. Then, R-hadrons produced in the squark decays were searched for in the data collected by DELPHI at the centre-of-mass energies of 189 to 208 GeV, corresponding to an overall integrated luminosity of 609 pb^{-1}. The observed number of events is in agreement with the Standard Model predictions. Limits at 95% confidence level are derived on the squark masses from the excluded regions in the plane ($m_{\tilde{\mathrm{q}}_1}$,$m_{\tilde{\mathrm{g}}}$):

$m_{\tilde{\mathrm{t}}_1} > 90$ GeV/c^2, and $m_{\tilde{\mathrm{b}}_1} > 96$ GeV/c^2 for purely left squarks.
$m_{\tilde{\mathrm{t}}_1} > 87$ GeV/c^2, and $m_{\tilde{\mathrm{b}}_1} > 82$ GeV/c^2 independent of the mixing angle.

(Submitted to Eur.Phys. J. C)

J.Abdallah[24], P.Abreu[22], W.Adam[50], P.Adzic[11], T.Albrecht[17], T.Alderweireld[2], R.Alemany-Fernandez[8], T.Allmendinger[17], P.P.Allport[23], U.Amaldi[28], N.Amapane[44], S.Amato[47], E.Anashkin[35], A.Andreazza[27], S.Andringa[22], N.Anjos[22], P.Antilogus[26], W-D.Apel[17], Y.Arnoud[14], S.Ask[25], B.Asman[43], J.E.Augustin[24], A.Augustinus[8], P.Baillon[8], A.Ballestrero[45], P.Bambade[20], R.Barbier[26], D.Bardin[16], G.Barker[17], A.Baroncelli[38], M.Battaglia[8], M.Baubillier[24], K-H.Becks[52], M.Begalli[6], A.Behrmann[52], E.Ben-Haim[20], N.Benekos[31], A.Benvenuti[5], C.Berat[14], M.Berggren[24], L.Berntzon[43], D.Bertrand[2], M.Besancon[39], N.Besson[39], D.Bloch[9], M.Blom[30], M.Bluj[51], M.Bonesini[28], M.Boonekamp[39], P.S.L.Booth[23], G.Borisov[21], O.Botner[48], B.Bouquet[20], T.J.V.Bowcock[23], I.Boyko[16], M.Bracko[42], R.Brenner[48], E.Brodet[34], P.Bruckman[18], J.M.Brunet[7], L.Bugge[32], P.Buschmann[52], M.Calvi[28], T.Camporesi[8], V.Canale[37], F.Carena[8], N.Castro[22], F.Cavallo[5], M.Chapkin[41], Ph.Charpentier[8], P.Checchia[35], R.Chierici[8], P.Chliapnikov[41], J.Chudoba[8], S.U.Chung[8], K.Cieslik[18], P.Collins[8], R.Contri[13], G.Cosme[20], F.Cossutti[46], M.J.Costa[49], B.Crawley[1], D.Crennell[36], J.Cuevas[33], J.D'Hondt[2], J.Dalmau[43], T.da Silva[47], W.Da Silva[24], G.Della Ricca[46], A.De Angelis[46], W.De Boer[17], C.De Clercq[2], B.De Lotto[46], N.De Maria[44], A.De Min[35], L.de Paula[47], L.Di Ciaccio[37], A.Di Simone[38], K.Doroba[51], J.Drees[52,8], M.Dris[31], G.Eigen[4], T.Ekelof[48], M.Ellert[48], M.Elsing[8], M.C.Espirito Santo[8], G.Fanourakis[11], D.Fassouliotis[11,3], M.Feindt[17], J.Fernandez[40], A.Ferrer[49], F.Ferro[13], U.Flagmeyer[52], H.Foeth[8], E.Fokitis[31], F.Fulda-Quenzer[20], J.Fuster[49], M.Gandelman[47], C.Garcia[49], Ph.Gavillet[8], E.Gazis[31], T.Geralis[11], R.Gokieli[8,51], B.Golob[42], G.Gomez-Ceballos[40], P.Goncalves[22], E.Graziani[38], G.Grosdidier[20], K.Grzelak[51], J.Guy[36], C.Haag[17], A.Hallgren[48], K.Hamacher[52], K.Hamilton[34], J.Hansen[32], S.Haug[32], F.Hauler[17], V.Hedberg[25], M.Hennecke[17], H.Herr[8], J.Hoffman[51], S-O.Holmgren[43], P.J.Holt[8], M.A.Houlden[23], K.Hultqvist[43], J.N.Jackson[23], G.Jarlskog[25], P.Jarry[39], D.Jeans[34], E.K.Johansson[43], P.D.Johansson[43], P.Jonsson[26], C.Joram[8], L.Jungermann[17], F.Kapusta[24], S.Katsanevas[26], E.Katsoufis[31], G.Kernel[42], B.P.Kersevan[8,42], A.Kiiskinen[15], B.T.King[23], N.J.Kjaer[8], P.Kluit[30], P.Kokkinias[11], C.Kourkoumelis[3], O.Kouznetsov[16], Z.Krumstein[16], M.Kucharczyk[18], J.Lamsa[1], G.Leder[50], F.Ledroit[14], L.Leinonen[43], R.Leitner[29], J.Lemonne[2], V.Lepeltier[20], T.Lesiak[18], W.Liebig[52], D.Liko[50], A.Lipniacka[43], J.H.Lopes[47], J.M.Lopez[33], D.Loukas[11], P.Lutz[39], L.Lyons[34], J.MacNaughton[50], A.Malek[52], S.Maltezos[31], F.Mandl[50], J.Marco[40], R.Marco[40], B.Marechal[47], M.Margoni[35], J-C.Marin[8], C.Mariotti[8], A.Markou[11], C.Martinez-Rivero[40], J.Masik[12], N.Mastroyiannopoulos[11], F.Matorras[40], C.Matteuzzi[28], F.Mazzucato[35], M.Mazzucato[35], R.Mc Nulty[23], C.Meroni[27], W.T.Meyer[1], E.Migliore[44], W.Mitaroff[50], U.Mjoernmark[25], T.Moa[43], M.Moch[17], K.Moenig[8,10], R.Monge[13], J.Montenegro[30], D.Moraes[47], S.Moreno[22], P.Morettini[13], U.Mueller[52], K.Muenich[52], M.Mulders[30], L.Mundim[6], W.Murray[36], B.Muryn[19], G.Myatt[34], T.Myklebust[32], M.Nassiakou[11], F.Navarria[5], K.Nawrocki[51], R.Nicolaidou[39], M.Nikolenko[16,9], A.Oblakowska-Mucha[19], V.Obraztsov[41], A.Olshevski[16], A.Onofre[22], R.Orava[15], K.Osterberg[15], A.Ouraou[39], A.Oyanguren[49], M.Paganoni[28], S.Paiano[5], J.P.Palacios[23], H.Palka[18], Th.D.Papadopoulou[31], L.Pape[8], C.Parkes[23], F.Parodi[13], U.Parzefall[8], A.Passeri[38], O.Passon[52], L.Peralta[22], V.Perepelitsa[49], A.Perrotta[5], A.Petrolini[13], J.Piedra[40], L.Pieri[38], F.Pierre[39], M.Pimenta[22], E.Piotto[8], T.Podobnik[42], V.Poireau[39], M.E.Pol[6], G.Polok[18], P.Poropat[†46], V.Pozdniakov[16], N.Pukhaeva[2,16], A.Pullia[28], J.Rames[12], L.Ramler[17], A.Read[32], P.Rebecchi[8], J.Rehn[17], D.Reid[30], R.Reinhardt[52], P.Renton[34], F.Richard[20], J.Ridky[12], M.Rivero[40], D.Rodriguez[40], A.Romero[44], P.Ronchese[35], E.Rosenberg[1], P.Roudeau[20], T.Rovelli[5], V.Ruhlmann-Kleider[39], D.Ryabtchikov[41], A.Sadovsky[16], L.Salmi[15], J.Salt[49], A.Savoy-Navarro[24], U.Schwickerath[8], A.Segar[34], R.Sekulin[36], M.Siebel[52], A.Sisakian[16], G.Smadja[26], O.Smirnova[25], A.Sokolov[41], A.Sopczak[21], R.Sosnowski[51], T.Spassov[8], M.Stanitzki[17], A.Stocchi[20], J.Strauss[50], B.Stugu[4], M.Szczekowski[51], M.Szeptycka[51], T.Szumlak[19], T.Tabarelli[28], A.C.Taffard[23], F.Tegenfeldt[48], J.Timmermans[30], L.Tkatchev[16], M.Tobin[23], S.Todorovova[12], A.Tomaradze[8], B.Tome[22], A.Tonazzo[28], P.Tortosa[49], P.Travnicek[12], D.Treille[8], G.Tristram[7], M.Trochimczuk[51], C.Troncon[27], M-L.Turluer[39], I.A.Tyapkin[16], P.Tyapkin[16], S.Tzamarias[11], V.Uvarov[41], G.Valenti[5], P.Van Dam[30], J.Van Eldik[8], A.Van Lysebetten[2], N.van Remortel[2], I.Van Vulpen[30], G.Vegni[27], F.Veloso[22], W.Venus[36], F.Verbeure[2], P.Verdier[26], V.Verzi[37], D.Vilanova[39], L.Vitale[46], V.Vrba[12], H.Wahlen[52],

A.J.Washbrook[23], C.Weiser[17], D.Wicke[8], J.Wickens[2], G.Wilkinson[34], M.Winter[9], M.Witek[18], O.Yushchenko[41], A.Zalewska[18], P.Zalewski[51], D.Zavrtanik[42], N.I.Zimin[16], A.Zintchenko[16], M.Zupan[11]

[1]Department of Physics and Astronomy, Iowa State University, Ames IA 50011-3160, USA
[2]Physics Department, Universiteit Antwerpen, Universiteitsplein 1, B-2610 Antwerpen, Belgium
and IIHE, ULB-VUB, Pleinlaan 2, B-1050 Brussels, Belgium
and Faculté des Sciences, Univ. de l'Etat Mons, Av. Maistriau 19, B-7000 Mons, Belgium
[3]Physics Laboratory, University of Athens, Solonos Str. 104, GR-10680 Athens, Greece
[4]Department of Physics, University of Bergen, Allégaten 55, NO-5007 Bergen, Norway
[5]Dipartimento di Fisica, Università di Bologna and INFN, Via Irnerio 46, IT-40126 Bologna, Italy
[6]Centro Brasileiro de Pesquisas Físicas, rua Xavier Sigaud 150, BR-22290 Rio de Janeiro, Brazil
and Depto. de Física, Pont. Univ. Católica, C.P. 38071 BR-22453 Rio de Janeiro, Brazil
and Inst. de Física, Univ. Estadual do Rio de Janeiro, rua São Francisco Xavier 524, Rio de Janeiro, Brazil
[7]Collège de France, Lab. de Physique Corpusculaire, IN2P3-CNRS, FR-75231 Paris Cedex 05, France
[8]CERN, CH-1211 Geneva 23, Switzerland
[9]Institut de Recherches Subatomiques, IN2P3 - CNRS/ULP - BP20, FR-67037 Strasbourg Cedex, France
[10]Now at DESY-Zeuthen, Platanenallee 6, D-15735 Zeuthen, Germany
[11]Institute of Nuclear Physics, N.C.S.R. Demokritos, P.O. Box 60228, GR-15310 Athens, Greece
[12]FZU, Inst. of Phys. of the C.A.S. High Energy Physics Division, Na Slovance 2, CZ-180 40, Praha 8, Czech Republic
[13]Dipartimento di Fisica, Università di Genova and INFN, Via Dodecaneso 33, IT-16146 Genova, Italy
[14]Institut des Sciences Nucléaires, IN2P3-CNRS, Université de Grenoble 1, FR-38026 Grenoble Cedex, France
[15]Helsinki Institute of Physics, HIP, P.O. Box 9, FI-00014 Helsinki, Finland
[16]Joint Institute for Nuclear Research, Dubna, Head Post Office, P.O. Box 79, RU-101 000 Moscow, Russian Federation
[17]Institut für Experimentelle Kernphysik, Universität Karlsruhe, Postfach 6980, DE-76128 Karlsruhe, Germany
[18]Institute of Nuclear Physics,Ul. Kawiory 26a, PL-30055 Krakow, Poland
[19]Faculty of Physics and Nuclear Techniques, University of Mining and Metallurgy, PL-30055 Krakow, Poland
[20]Université de Paris-Sud, Lab. de l'Accélérateur Linéaire, IN2P3-CNRS, Bât. 200, FR-91405 Orsay Cedex, France
[21]School of Physics and Chemistry, University of Lancaster, Lancaster LA1 4YB, UK
[22]LIP, IST, FCUL - Av. Elias Garcia, 14-1^{o}, PT-1000 Lisboa Codex, Portugal
[23]Department of Physics, University of Liverpool, P.O. Box 147, Liverpool L69 3BX, UK
[24]LPNHE, IN2P3-CNRS, Univ. Paris VI et VII, Tour 33 (RdC), 4 place Jussieu, FR-75252 Paris Cedex 05, France
[25]Department of Physics, University of Lund, Sölvegatan 14, SE-223 63 Lund, Sweden
[26]Université Claude Bernard de Lyon, IPNL, IN2P3-CNRS, FR-69622 Villeurbanne Cedex, France
[27]Dipartimento di Fisica, Università di Milano and INFN-MILANO, Via Celoria 16, IT-20133 Milan, Italy
[28]Dipartimento di Fisica, Univ. di Milano-Bicocca and INFN-MILANO, Piazza della Scienza 2, IT-20126 Milan, Italy
[29]IPNP of MFF, Charles Univ., Areal MFF, V Holesovickach 2, CZ-180 00, Praha 8, Czech Republic
[30]NIKHEF, Postbus 41882, NL-1009 DB Amsterdam, The Netherlands
[31]National Technical University, Physics Department, Zografou Campus, GR-15773 Athens, Greece
[32]Physics Department, University of Oslo, Blindern, NO-0316 Oslo, Norway
[33]Dpto. Fisica, Univ. Oviedo, Avda. Calvo Sotelo s/n, ES-33007 Oviedo, Spain
[34]Department of Physics, University of Oxford, Keble Road, Oxford OX1 3RH, UK
[35]Dipartimento di Fisica, Università di Padova and INFN, Via Marzolo 8, IT-35131 Padua, Italy
[36]Rutherford Appleton Laboratory, Chilton, Didcot OX11 OQX, UK
[37]Dipartimento di Fisica, Università di Roma II and INFN, Tor Vergata, IT-00173 Rome, Italy
[38]Dipartimento di Fisica, Università di Roma III and INFN, Via della Vasca Navale 84, IT-00146 Rome, Italy
[39]DAPNIA/Service de Physique des Particules, CEA-Saclay, FR-91191 Gif-sur-Yvette Cedex, France
[40]Instituto de Fisica de Cantabria (CSIC-UC), Avda. los Castros s/n, ES-39006 Santander, Spain
[41]Inst. for High Energy Physics, Serpukov P.O. Box 35, Protvino, (Moscow Region), Russian Federation
[42]J. Stefan Institute, Jamova 39, SI-1000 Ljubljana, Slovenia and Laboratory for Astroparticle Physics,
Nova Gorica Polytechnic, Kostanjeviska 16a, SI-5000 Nova Gorica, Slovenia,
and Department of Physics, University of Ljubljana, SI-1000 Ljubljana, Slovenia
[43]Fysikum, Stockholm University, Box 6730, SE-113 85 Stockholm, Sweden
[44]Dipartimento di Fisica Sperimentale, Università di Torino and INFN, Via P. Giuria 1, IT-10125 Turin, Italy
[45]INFN,Sezione di Torino, and Dipartimento di Fisica Teorica, Università di Torino, Via P. Giuria 1,
IT-10125 Turin, Italy
[46]Dipartimento di Fisica, Università di Trieste and INFN, Via A. Valerio 2, IT-34127 Trieste, Italy
and Istituto di Fisica, Università di Udine, IT-33100 Udine, Italy
[47]Univ. Federal do Rio de Janeiro, C.P. 68528 Cidade Univ., Ilha do Fundão BR-21945-970 Rio de Janeiro, Brazil
[48]Department of Radiation Sciences, University of Uppsala, P.O. Box 535, SE-751 21 Uppsala, Sweden
[49]IFIC, Valencia-CSIC, and D.F.A.M.N., U. de Valencia, Avda. Dr. Moliner 50, ES-46100 Burjassot (Valencia), Spain
[50]Institut für Hochenergiephysik, Österr. Akad. d. Wissensch., Nikolsdorfergasse 18, AT-1050 Vienna, Austria
[51]Inst. Nuclear Studies and University of Warsaw, Ul. Hoza 69, PL-00681 Warsaw, Poland
[52]Fachbereich Physik, University of Wuppertal, Postfach 100 127, DE-42097 Wuppertal, Germany
† deceased

1 Introduction

In minimal supergravity supersymmetry models (mSUGRA), the gaugino masses (M_i) are usually supposed to evolve from a common value $m_{1/2}$ at the GUT scale. In such models, the M_i are proportional to the corresponding coupling constants (g_i) and the gluino is naturally heavier than the other gauginos at the electroweak scale.

$$\frac{M_1}{g_1^2} = \frac{M_2}{g_2^2} = \frac{M_3}{g_3^2} \quad \text{that is,} \quad M_1 : M_2 : M_3 \sim 1 : 2 : 7$$

Nevertheless, models exist where the M_i do not follow this relation. M_3 could be lighter than the other gaugino masses [1], and in this case, the gluino is the Lightest Supersymmetric Particle (LSP). For example there is a particular Gauge Mediated Supersymmetry Breaking model (GMSB) [2] where the gluino can either be the LSP or the next to lightest supersymmetric particle (NLSP) with a gravitino LSP. In the latter case, the lifetime of the gluino would ever be sufficiently large to consider the gluino as a stable particle for collider physic. If R-parity is assumed, the gluino is stable in all these models and it should hadronize to form R-hadrons because of color confinement.

The gluino has been intensively searched for in hadron collisions in various decay channels [3]. However, the limit obtained ($m_{\tilde{g}} > 173$ GeV/c^2 for $m_{\tilde{g}} = m_{\tilde{q}}$) does not apply to a stable gluino. For this model, it has been shown that CDF run I data could not constrain a stable gluino with mass lower than 35 GeV/c^2 [1,2]. On the other hand, the gluino mass could be much larger than it is in the so-called light gluino scenario [4], which seems to be excluded by the measurement of the triple gluon coupling and of the four-jet rates at LEP [5].

A pair of gluinos can be produced in the splitting of a gluon. Figure 1 shows the Feynman diagram of this process and the corresponding cross-sections at centre-of-mass energies of 91.2 GeV (LEP1) and of 200 GeV (LEP2). The production rate is too low at LEP2, and LEP1 data must be analysed to be sensitive to this process. In this channel, the gluino does not originate from the decay of another sparticle, so it can be produced even if the other supersymmetric particles are not accessible.

Gluinos can also be produced from other sparticle decays. $\widetilde{\mathrm{q}}_L$ and $\widetilde{\mathrm{q}}_R$ are the supersymmetric partners of the left-handed and right handed quarks. With large Yukawa coupling running and important off-diagonal terms the supersymmetric partners of top and bottom quarks are the most probable candidates for the charged lightest supersymmetric particle. The squark mass eigenstates are parametrised by a mixing angle $\theta_{\tilde{\mathrm{q}}}$. The lighter squark is given by $\widetilde{\mathrm{q}}_1 = \widetilde{\mathrm{q}}_L \sin\theta_{\tilde{q}} + \widetilde{\mathrm{q}}_R \cos\theta_{\tilde{q}}$. The stop ($\widetilde{\mathrm{t}}_1$) and the sbottom ($\widetilde{\mathrm{b}}_1$) could be pair-produced at LEP via $\mathrm{e^+e^-}$ annihilation into Z^0/γ. A squark mixing angle equal to zero leads to the maximal squark pair production cross-section, while the minimal cross-sections are obtained for a mixing angle of 56° for the stop and of 68° for the sbottom. For these particular angles, the $\mathrm{Z}^0 - \widetilde{\mathrm{q}}_1 - \bar{\widetilde{\mathrm{q}}}_1$ coupling is suppressed. This paper also describes the search for R-hadrons from stop and sbottom decays at LEP2. The dominant decay of the stop and of the sbottom are $\widetilde{\mathrm{t}}_1 \rightarrow \mathrm{c}\widetilde{\mathrm{g}}$ and $\widetilde{\mathrm{b}}_1 \rightarrow \mathrm{b}\widetilde{\mathrm{g}}$ [6] when the gluino is lighter than the squarks, as in the stable gluino scenario. The branching ratios of these decay channels were taken to be 100%. Figure 2 shows the squark production and decay diagrams.

DELPHI data collected in 1994 at a centre-of-mass energy of 91.2 GeV were used to search for the process $\mathrm{e^+e^-} \rightarrow \mathrm{q\bar{q}}\widetilde{\mathrm{g}}\widetilde{\mathrm{g}}$. Then, stop and sbottom squarks were searched for in DELPHI data collected from 1998 to 2000 at centre-of-mass energies ranging from 189

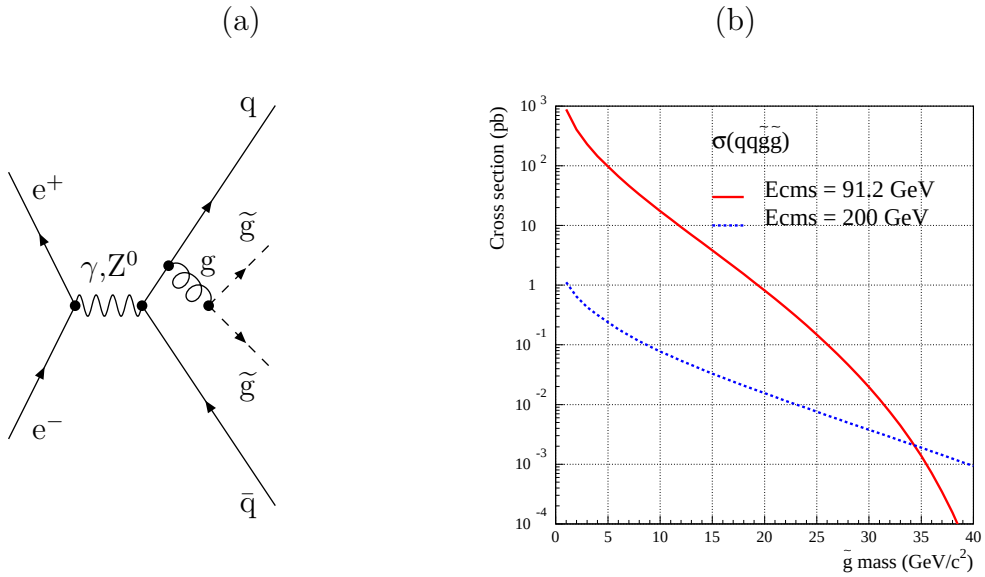

Figure 1: (a) Gluon splitting into a pair of gluinos. (b) Comparison of the cross-section (pb) of this process at centre-of-mass energies of 91.2 GeV (LEP1) and of 200 GeV (LEP2).

to 208 GeV. The three analyses presented in this paper are therefore searches for:

$$\begin{cases} e^+e^- \rightarrow q\bar{q}g \rightarrow q\bar{q}\widetilde{g}\widetilde{g} \\ e^+e^- \rightarrow \widetilde{t}_1\bar{\widetilde{t}}_1 \rightarrow c\widetilde{g}\bar{c}\widetilde{g} \\ e^+e^- \rightarrow \widetilde{b}_1\bar{\widetilde{b}}_1 \rightarrow b\widetilde{g}\bar{b}\widetilde{g} \end{cases}$$

all giving the same topology of two standard jets plus two gluino jets. The gluino could either fragment to neutral R° states ($\widetilde{g}g$, $\widetilde{g}u\bar{u}$, ...) or to charged $R^{\pm}$ states ($\widetilde{g}u\bar{d}$,...). If P is the probability that a gluino fragments to a charged R-hadron, then for $P = 1$, R-hadrons are identified by an anomalous ionizing energy loss in the tracking chambers, and for $P = 0$, the gluino hadronizes into neutral states which reach the calorimeters where they deposit a part of their energy. The missing energy carried away by the LSP is reduced compared with usual SUSY models with R-parity conservation. For neutral R-hadrons, the estimate of the experimental sensitivity depends on the model used to calculate the energy loss in the calorimeters.

2 The DELPHI detector

The description of the DELPHI detector and its performance can be found in references [7,8]. We only summarize here the parts relevant to the analysis.

Charged particles are reconstructed in a 1.2 T magnetic field by a system of cylindrical tracking detectors. The closest to the beam is the Vertex Detector (VD) which consists of three cylindrical layers of silicon detectors at radii 6.3 cm, 9.0 cm and 11.0 cm. They measure coordinates in the $R\phi$ plane [1]. In addition, the inner and the outer layers are double-sided giving also a z measurement. VD is the barrel part of the Silicon Tracker

[1] The DELPHI coordinate system is defined with z along the e^- beam direction; θ and ϕ are the polar and azimuthal angles and R is the radial distance from the z axis.

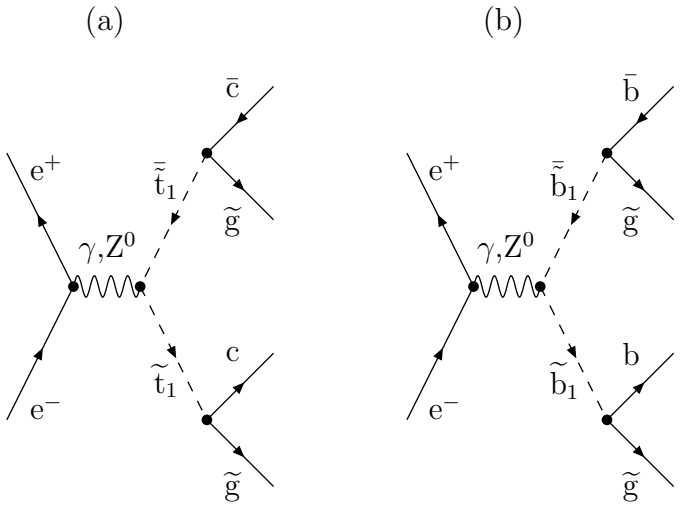

Figure 2: Stop (a) and sbottom (b) production and decay at LEP2.

(ST), which extends the polar angle acceptance down to 10 degrees. The Inner Detector (ID) is a drift chamber with inner radius 12 cm and outer radius 22 cm covering polar angles between 15° and 165°. The principal tracking detector of DELPHI is the Time Projection Chamber (TPC). It is a cylinder of 30 cm inner radius, 122 cm outer radius and 2.7 m length. Each end-plate is divided into 6 sectors, with 192 sense wires to allow the dE/dx measurement, and with 16 circular pad rows which provide 3-dimensional track reconstruction. The TPC covers polar angles from 20° to 160°. Finally, the Outer Detector (OD) consists of drift cells at radii between 192 cm and 208 cm, covering polar angles between 43° and 137°. In addition, two planes of drift chambers perpendicular to the beam axis (Forward Chambers A and B) are installed in the endcaps covering polar angles $11° < \theta < 33°$ and $147° < \theta < 169°$.

The electromagnetic calorimeters are the High density Projection Chamber (HPC) in the barrel region ($40° < \theta < 140°$) and the Forward Electromagnetic Calorimeter (FEMC) in the endcaps ($11° < \theta < 36°$ and $144° < \theta < 169°$). In the forward and backward regions, the Scintillator TIle Calorimeter (STIC) extends the coverage down to 1.66° from the beam axis. The number of radiation lengths are respectively 18, 20 and 27 in the HPC, the FEMC and the STIC. In the gap between the HPC and the FEMC, hermeticity taggers made of single layer scintillator-lead counters are used to veto events with electromagnetic particles which would otherwise escape detection. Between the HPC modules, gaps at $\theta = 90°$ and gaps in ϕ are also instrumented with such taggers. Finally, the hadron calorimeter (HCAL) covers polar angle between $11° < \theta < 169°$. The iron thickness in the HCAL is 110 cm which corresponds to 6.6 nuclear interaction lengths.

3 Data and Monte Carlo samples

The total integrated luminosity collected by the DELPHI detector in 1994 at the Z^0 peak ($\sqrt{s} = 91.2$ GeV) was 46 pb^{-1}. It corresponded to around 1.6 million hadronic Z^0 events. The Standard Model hadronic background was estimated with the JETSET 7.3 [9] program tuned to reproduce LEP1 data [10]. The program described in [1] was used to simulate the $e^+e^- \to q\bar{q}\tilde{g}\tilde{g}$ signal.

At LEP2, the total integrated luminosity collected by the DELPHI detector at centre-of-mass energies from 189 to 208 GeV was 609 pb^{-1}. In September 2000, one of the twelve TPC sectors (sector 6) stopped functioning. About 60 pb^{-1} of data were collected without that sector until the end of the data taking. The reconstruction programs were modified to allow the analysis of the data taken with the DELPHI TPC not fully operational. After this modification, there was only a small degradation of the performance of the tracking. The data collected in year 2000 were divided in centre-of-mass energy windows to optimize the analysis sensitivity. Table 1 summarizes the LEP2 data samples used in the analysis.

Year	$<\sqrt{s}>$ (GeV) Data	$\sqrt{s}$ (GeV) Simulated MC	Integrated luminosity (pb^{-1})
1998	188.6	189	158.0
1999	191.6	192	25.9
	195.6	196	76.4
	199.6	200	83.4
	201.6	202	40.6
2000	204.8	204	78.1
	206.6	206	78.5
	208.1	208	7.3
2000(*)	206.5	206.7	60.6

Table 1: Total integrated luminosity as a function of the centre-of-mass energy of the LEP2 analysed data samples. The third column shows the centre-of-mass energy of the simulated events. (*) indicates the data collected by DELPHI in 2000 without the sector 6 of the TPC.

The e^+e^- interactions leading to four-fermion final states were generated using EXCALIBUR [11]. GRC4F [12] was used to simulate the processes $e^+e^- \to e\nu q\bar{q}$ and $e^+e^- \to Z^o ee$ with electrons emitted at polar angles lower than the cut imposed in EXCALIBUR. The two-fermion final states were generated with PYTHIA [9] for $e^+e^- \to q\bar{q}(n\gamma)$, KORALZ [13] for $e^+e^- \to \tau^+\tau^-(\gamma)$, $e^+e^- \to \mu^+\mu^-(\gamma)$, $e^+e^- \to \nu\nu(\gamma)$, and BHWIDE [14] for $e^+e^- \to e^+e^-(\gamma)$. PYTHIA 6.143 [15] was used to simulate $\gamma\gamma$ interactions leading to hadronic final states. BDKRC [16] was used for $\gamma\gamma$ interactions leading to leptonic final states. In all cases, the final hadronization of the particles was performed with JETSET [9].

The flavour changing decay $\widetilde{t}_1 \to c\widetilde{g}$ goes through one-loop diagrams. Therefore, $\widetilde{t}_1$ is expected to be long-lived and to hadronize before its decay. A modified version of the SUSYGEN [17] generator was used to simulate this process. Special care was taken to introduce hard gluon radiation off the scalar stop at the matrix-element level and to treat the stop hadronization as a non-perturbative strong interaction effect. A detailed description of this hadronization model can be found in [18]. Such a model, based on the Peterson function [19], was also used to perform the gluino hadronization into R-hadrons. SUSYGEN has also been modified to perform the sbottom decay into $b\widetilde{g}$. Figure 3 summarizes the stop and sbottom production and the fragmentation steps. The final hadronization was performed using JETSET [9].

The Monte Carlo samples used to simulate the Standard Model processes and the supersymmetric signals were passed through DELSIM [20], the program simulating the

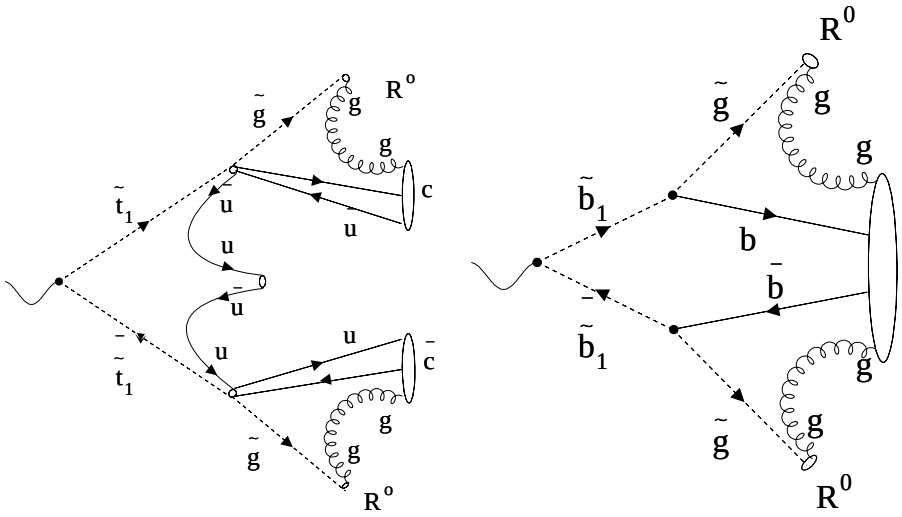

Figure 3: Production and decay of the stop and sbottom squarks. Ellipses indicate the color singlet and the color string stretched between the partons.

full DELPHI detector response. They were subsequently processed with the same reconstruction program as the real data. The number of generated events was always several times higher than the number expected for the integrated luminosity collected.

4 R-hadron simulation

In the analysis, two generic R-hadron states were considered: one charged denoted $\mathrm{R}^{\pm}$ and one neutral, R°, which corresponds to the glueballino, a $\widetilde{\mathrm{g}}\mathrm{g}$ state. It is important to understand how an R° would manifest itself in the detector. We refer to the results of reference [1]. The energy loss in the scattering on a nucleon $\mathrm{R}^{\circ}\mathrm{N} \to \mathrm{R}^{\circ}\mathrm{X}$ is given by:

$$\Delta E = \frac{m_X^2 - m_N^2 + |t|}{2m_N}$$

where $|t|$ is the usual momentum transfer invariant for the R° and m_X is the mass of the system produced in the $\mathrm{R}^{\circ}\mathrm{N} \to \mathrm{R}^{\circ}\mathrm{X}$ collision. The average energy loss in the reaction $\mathrm{R}^{\circ}\mathrm{N} \to \mathrm{R}^{\circ}\mathrm{X}$ is then given by:

$$\langle \Delta E \rangle = \frac{\int_{m_N}^{\sqrt{s}-m_{R^\circ}} dm_X \int_{|t|_{\min}(m_X)}^{|t|_{\max}(m_X)} d|t| \, \Delta E \frac{d\sigma}{d|t|dm_X}}{\int_{m_N}^{\sqrt{s}-m_{R^\circ}} dm_X \int_{|t|_{\min}(m_X)}^{|t|_{\max}(m_X)} d|t| \frac{d\sigma}{d|t|dm_X}}$$

where $s = M_{R^\circ}^2 + m_N^2 + 2\gamma M_{R^\circ} m_N$ describes the collision energy. The following functions are defined:

$$\begin{cases} \gamma & = & (1-\beta^2)^{-1/2} \\ |t|_{\min,\max}(m_X) & = & 2[E(m_N)E(m_X) \mp p(m_N)p(m_X) - M_{R^\circ}^2] \\ E(m) & = & (s + M_{R^\circ}^2 - m^2)/(2\sqrt{s}) \\ p(m) & = & \lambda^{1/2}(s, M_{R^\circ}^2, m^2)/(2\sqrt{s}) \\ \lambda(a,b,c) & = & a^2 + b^2 + c^2 - 2(ab + ac + bc) \end{cases}$$

From the results of studies in [1], the differential cross-section $\frac{d\sigma}{d|t|dm_X}$ is taken as:

$$\frac{d\sigma}{d|t|dm_X} \propto \begin{cases} 1, \text{ if } |t| \leq 1 \text{ GeV}^2 \\ 0, \text{ if } |t| > 1 \text{ GeV}^2 \end{cases}$$

The average number of collisions of an R° particle in the calorimeters is given by the depth of the calorimeter in units of equivalent iron interaction lengths, λ_T. In DELPHI, the electromagnetic calorimeter's thickness represents around 1 λ_T while this value is 6.6 λ_T for the hadronic calorimeter. We have adopted a correction factor for the interaction length of 9/16 as suggested in reference [1]: a factor $C_A/C_F = 9/4$ comes from the colour octet nature of the R° constituents increasing the $\sigma_{R^\circ N}$ cross-section as compared to $\sigma_{\pi N}$, while a factor $\langle r^2_{R^\circ}\rangle/\langle r^2_\pi\rangle = 1/4$ takes into account the relative size of the R-hadrons as compared to standard hadrons. On average, neutral R-hadrons should undergo 4.3 collisions in DELPHI calorimeters. Figure 4 shows the total energy loss by an R° after 4 collisions in iron.

The difficulty in separating the signal of a neutral R-hadron from the background increases with the amount of energy lost in the calorimeters. The choice of the interaction model made here is conservative in this respect. The R° scatters were subsequently treated in the DELPHI detector simulation as K^0_L with the energy that the R° should deposit in four collisions according to the above formula.

The charged R-hadrons were treated as heavy muons to reproduce the anomalous dE/dx signature. In this case, only the tracking information was used to calculate the R-hadron momentum.

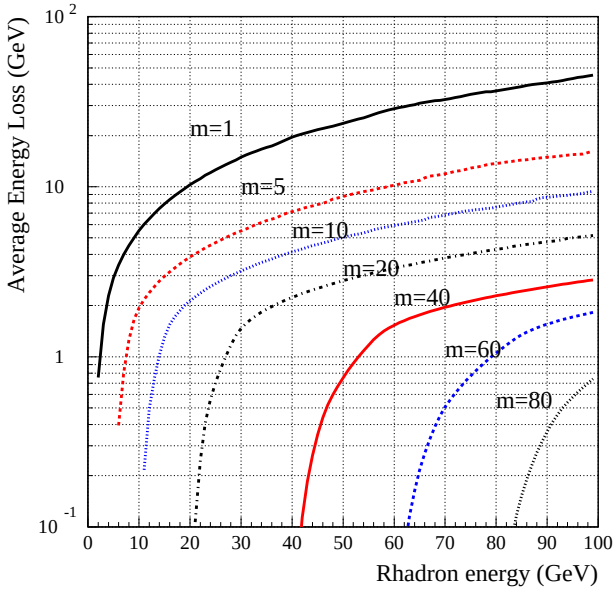

Figure 4: Average energy loss by neutral R-hadrons in the DELPHI calorimeters as a function of their initial energy for different mass cases.

5 Particle Identification and analysis method

5.1 Particle Identification and event preselection

Particle selection was identical for LEP1 and LEP2 data. Reconstructed charged particles were required to have momenta above 100 MeV/c with $\Delta p/p < 1$, where Δp is the momentum error, and impact parameter below 5 cm in the transverse plane and below 10 cm/ $\sin\theta$ in the beam direction. More stringent cuts were applied for tracks without TPC information. A cluster in the calorimeters was selected as a neutral particle if not associated to a charged particle and if the cluster energy was greater than 500 MeV in the HPC, 400 MeV in the FEMC, 300 MeV in the STIC or 900 MeV in the HAC. Particles were then clustered into jets with the DURHAM algorithm [21]. b-quarks were tagged using a probabilistic method based on the impact parameters of tracks with respect to the main vertex. A combined b-tagging variable was defined by including the properties of secondary vertices [22].

Events were then kept if there were at least two charged particles, and at least one with a transverse momentum above 1.5 GeV/c, and if the transverse energy [2] exceeded 4 GeV.

5.2 Neural networks

A neural network allows one discriminating variable to be constructed from the set of variables given as input. The form used here contains three layers of nodes: the input layer where each neuron corresponds to a discriminating variable, the hidden layer, and the output layer which is the response of the neural network. The layers were connected in a "feed forward" architecture. The back-propagation algorithm was used to train the network with simulated events. This entails minimising a χ^2 to adjust the neurons' weights and connections. An independent validation sample was also used not to overtrain the network. The outputs of neural networks were used to isolate events containing two neutral R-hadrons at LEP2.

5.3 General description of the analyses

The LEP1 and LEP2 data analyses have all the same final states which consists of two jets and two gluino jets. Depending on the probability P that the gluino hadronizes into a charged R-hadron, three topologies are possible:

- charged: $e^+e^- \rightarrow q\bar{q}R^{\pm}R^{\pm}$
- mixed: $e^+e^- \rightarrow q\bar{q}R^{\pm}R^{\circ}$
- neutral: $e^+e^- \rightarrow q\bar{q}R^{\circ}R^{\circ}$

For LEP1 data, the search analyses corresponding to the charged and the mixed topologies were identical, while they were optimised separately for LEP2 data. For these two topologies, the LEP1 and LEP2 analyses were only based on anomalous ionizing energy loss, and no quark tagging was applied.

For the neutral topology, LEP1 data were analyzed using sequential cuts without trying to tag the quark flavor. Since there are b-quarks in the final state of the sbottom decay, the b-quark tagging improves the isolation of this signal from the Standard Model backgrounds. Therefore, the b-tagging variable was used in the stop and sbottom search

[2] The transverse energy is defined as the sum of $\sqrt{p_T^2 + m^2}$ over all particles; p_T is the transverse momentum.

analyses at LEP2 in the neutral topology. This variable was included into the neural networks which were used to isolate the stop and the sbottom signals.

6 Search for a stable gluino at LEP1

6.1 Search for $q\bar{q}R^{\pm}R^{\pm}$ and $q\bar{q}R^{\pm}R^{\circ}$ events

The same analysis based on the dE/dx measurement was performed to identify $q\bar{q}R^{\pm}R^{\pm}$ and $q\bar{q}R^{\pm}R^{\circ}$ events.

In the preselection step, events were required to contain at least 5 charged particles. At least one of these had to satisfy the following conditions. The track was required to be reconstructed including a TPC track element and to have a momentum above 10 GeV/c. At least 80 wires of the TPC were required to have been included in the dE/dx measurement. The dE/dx had to be either greater than 1.8 mip (units of energy loss for a minimum ionizing particle), or less than the dE/dx expected for a particle of mass equal to 1 GeV/c^2. The Y_{23} variable is the y_{cut} value in the DURHAM algorithm for which the number of jets changes between two and three. $q\bar{q}R^{\pm}R^{\pm}$ and $q\bar{q}R^{\pm}R^{\circ}$ events contain three or four jets. Thus, Y_{23} was required to be less than 0.01. Figure 5 shows a comparison between simulated and real data at this level.

A $R^{\pm}$ candidate had to satisfy the following conditions: it had to be reconstructed with the VD, the ID and the TPC detectors, and the dE/dx measurement had to be based on at least 80 wires of the TPC. In addition, the energy of the other particles in a 15° cone around the $R^{\pm}$ candidate had to be less than 2 GeV. Finally, its associated electromagnetic energy had to be less than 5 GeV.

The final selection was performed by cuts in the plane (P,dE/dx). Figure 6 shows the expected dE/dx as a function of the particle momentum. The analysis was separated into two mass windows:

- $m_{\tilde{g}} < 14$ GeV/c^2:
  Here, charged R-hadrons were identified by low dE/dx values. The $R^{\pm}$ candidates were selected if their momentum was greater than 15 GeV/c, and if their dE/dx was less than the dE/dx expected for a particle of mass equal to 3 GeV/c^2.
- $m_{\tilde{g}} \geq 14$ GeV/c^2:
  In this mass window, R-hadrons were identified by high dE/dx values. The $R^{\pm}$ candidates were selected if their dE/dx was greater than 2 mip.

The final selection was performed by requiring at least one charged R-hadron candidate in either mass window. Table 2 contains the number of events selected after each cut of this analysis. For $m_{\tilde{g}} < 14$ GeV/c^2, 5 events were selected when 4.2 were expected. These numbers are 12 and 13.5 in the $m_{\tilde{g}} \geq 14$ GeV/c^2 mass window. Unlike the expected signal, all selected candidates in the data have only one particle with anomalous dE/dx. Figure 7 shows the signal detection efficiencies. For $q\bar{q}R^{\pm}R^{\pm}$, they ranged from a few percent for gluino masses close to 2 GeV/c^2 to around 50% for gluino masses of the order of 25 GeV/c^2. $q\bar{q}R^{\pm}R^{\circ}$ efficiencies were about half of the $q\bar{q}R^{\pm}R^{\pm}$ ones.

6.2 Search for $q\bar{q}R^{\circ}R^{\circ}$events

The search for $q\bar{q}R^{\circ}R^{\circ}$ events was performed at LEP1 with a sequential cut analysis. It was based on the search for the small part of missing energy carried away by the neutral R-hadrons. Hadronic events were first selected by requiring at least 5 charged particles.

After forcing the events into two jets, the acollinearity [3] was required to be greater than 20° to reduce the huge number of background Standard Model $Z^0 \to q\bar{q}$ events.

The following cuts were applied to reduce the number of hadronic $\gamma\gamma$ interactions. The number of tracks reconstructed with the TPC had to be greater than 4, and the energy of the particles with tracks reconstructed using only the VD and ID detectors had to be less than 20% of the total energy. The energies in 40° and 20° cones around the beam axis were required to be less than 40% and 10% of the total energy respectively. The transverse energy had to be greater than 20 GeV.

Hadronic events with missing energy were then selected in the barrel region of the detector. The visible mass was required to be less than 60 GeV/c^2. The thrust axis and the missing momentum had to point in the polar regions $[37°, 143°]$ and $[45°, 135°]$ respectively. Figure 8 shows a comparison between data and simulation at this level of the selection.

The Y_{23} quantity was then required to be less than 0.01 and events had to contain less than 20 charged particles. In order to reduce the number of events with two back-to-back jets, the acoplanarity [4] was required to be greater than 10° and the thrust to be less than 0.95. The final cut was bi-dimensional. The value of the variable $M_{jet1}/E_{jet1} + M_{jet2}/E_{jet2}$ was calculated from the two jets reconstructed with the DURHAM algorithm. Events were rejected if this variable was greater than 0.45 and if the acollinearity was less than 50°. Table 3 shows the number of events after each cut of the $q\bar{q}R^\circ R^\circ$ analysis. 12 events were selected in the data while 10.6 were expected in the hadronic background. Signal efficiencies as a function of the gluino mass are shown in figure 7. They ranged from a few percent for low gluino masses to around 20% for $m_{\tilde{g}} = 18$ GeV/c^2.

7 Search for a stable gluino at LEP2

7.1 Preselection

A common preselection for the charged and neutral R-hadron analyses was applied to reduce the background coming from soft $\gamma\gamma$ interactions. The cuts are the same for the stop and sbottom analysis at all centre-of-mass energies ranging from 189 to 208 GeV.

First, events were forced into two jets. To select hadronic events, the number of charged particles reconstructed with the TPC was required to be greater than three, and the energy in the STIC to be less than 70% of the total visible energy. The polar angle of the thrust axis had to be in the interval $[20°, 160°]$. Then, quality cuts were applied. The fraction of good tracks was defined as the ratio between the number of charged particles remaining after the track selection divided by this number before the selection. It had to be greater than 35%. In addition, the scalar sum of particle momenta reconstructed with the TPC was required to be greater than 55% of the total reconstructed energy and the number of charged particles to be greater than six. To remove radiative events, the energy of the most energetic neutral particle had to be less than 40 GeV. Table 4 contains the number of events after each of these cuts.

For the $q\bar{q}R^\pm R^\pm$ and $q\bar{q}R^\pm R^\circ$ analyses, charged R-hadron candidates were defined at this level. They had to be reconstructed with the VD, ID and TPC detectors and their momentum was required to be greater than 10 GeV/c. At least 80 sense wires of the TPC were required to have contributed to the measurement of their dE/dx. Their associated electromagnetic energy was required to be less than 5 GeV, and the energy of the other

[3] The acollinearity of two jets is defined as the complement of the angle between their directions.

[4] The acoplanarity of two jets is defined as the complement of the angle between their directions projected onto the plane perpendicular to z.

charged particles in a 15° cone around a candidate had to be less than 5 GeV. In 2000 , the dE/dx could not be used in sector 6 of the TPC for almost any of the data. For this sample, charged R-hadron candidates in this sector were removed.

7.2 Search for $q\bar{q}R^{\pm}R^{\pm}$ events

The search for $q\bar{q}R^{\pm}R^{\pm}$ events was exactly the same for the stop and the sbottom analyses. Events were selected if they contained at least two charged R-hadron candidates. Figure 9 shows the momentum and the dE/dx distribution of the selected $R^{\pm}$ candidates. Table 4 shows the number of selected events.

The analysis was then separated into three windows in gluino mass, and cuts in the plane (P,dE/dx) were applied:

- $m_{\tilde{g}} \leq 30$ GeV/c^2:
  events had to contain at least one charged R-hadron candidate with momentum greater than 20 GeV/c, and with dE/dx less than the dE/dx expected for a particle of mass equal to 3 GeV/c^2.
- 30 GeV/c^2 $< m_{\tilde{g}} <$ 60 GeV/c^2:
  events were selected if they contained at least two charged R-hadron candidates with dE/dx both greater than the dE/dx expected for a particle of mass equal to 30 GeV/c^2, and less than the dE/dx expected for a particle of mass equal to 60 GeV/c^2. Moreover, this dE/dx had also to be either less than the dE/dx expected for a particle of mass equal to 1 GeV/c^2, or greater than 1.8 mip.
- $m_{\tilde{g}} \geq 60$ GeV/c^2:
  events were kept if they contained at least two charged R-hadron candidates with dE/dx greater than the dE/dx expected for a particle of mass equal to 60 GeV/c^2.

In all LEP2 data which were analysed, no events were selected in any of these windows. The number of expected Standard Model background events were 0.115, 0.009 and 0.011 in the analyses for $m_{\tilde{g}} \leq 30$ GeV/c^2, 30 GeV/c^2 $< m_{\tilde{g}} <$ 60 GeV/c^2 and $m_{\tilde{g}} \geq 60$ GeV/c^2 respectively. Table 5 contains the number of events expected for the different centre-of-mass energies. Figure 10 shows the signal detection efficiencies near the kinematical limit ($m_{\tilde{q}_1} = 90$ GeV/c^2). The difference between stop and sbottom efficiencies is not large. The highest efficiencies were always obtained for high gluino masses, where the dE/dx is very high.

7.3 Search for $q\bar{q}R^{\pm}R^{\circ}$ events

The search for $q\bar{q}R^{\pm}R^{\circ}$ events was also the same for the stop and sbottom analyses. Events were selected if they contained at least one charged R-hadron candidate. Figure 11 shows the momentum and the dE/dx distribution of the selected $R^{\pm}$ candidates. Table 4 shows the number of selected events.

The analysis was then separated into three gluino mass windows, and cuts in the plane (P,dE/dx) were applied:

- $m_{\tilde{g}} \leq 30$ GeV/c^2:
  events had to contain at least one charged R-hadron candidate with momentum greater than 20 GeV/c, and with dE/dx less than the dE/dx expected for a particle of mass equal to 3 GeV/c^2.
- $m_{\tilde{g}} \geq 60$ GeV/c^2:
  events were kept if they contained at least one charged R-hadron candidate with

dE/dx greater than the dE/dx expected for a particle of mass equal to 60 GeV/c^2, and greater than 2 mip.

- 30 GeV/c^2 $< m_{\tilde{g}} <$ 60 GeV/c^2:
  events selected in either of the above windows (higher or lower $m_{\tilde{g}}$) were accepted.

Three, nine and six events were selected in the mass windows $m_{\tilde{g}} \leq$ 30 GeV/c^2, 30 GeV/c^2 $< m_{\tilde{g}} <$ 60 GeV/c^2 and $m_{\tilde{g}} \geq$ 60 GeV/c^2 respectively. The number of expected background events were 1.6, 8.2 and 6.6. All selected events in the data are more likely Standard Model instead than signal like. In particular, they do not follow any mass iso-curve in the (P,dE/dx) plane. Table 6 contains the number of selected events as a function of the centre-of-mass energy. Figure 12 shows the signal detection efficiencies near the kinematical limit ($m_{\tilde{q}_1} = 90$ GeV/c^2). The highest efficiencies were obtained for high gluino masses where the dE/dx is very high.

7.4 Search for $q\bar{q}R^{\circ}R^{\circ}$ events

After the preselection described in section 7.1, the transverse missing momentum was required to be greater than 4 GeV/c, the angle of the missing momentum had to point in the polar angle region $[20^{\circ}, 160^{\circ}]$, and the energy in a 40° cone around the beam axis was required to be less than 40% of the event energy. A veto algorithm was then applied based on the hermeticity taggers at polar angles close to 40° and 90°. Figures 13 and 14 show data Monte Carlo comparisons following this selection and table 7 gives the observed and expected event numbers at the different steps.

The stop and sbottom analyses were then separated for different ranges of the mass difference Δm between the squark and the gluino:

- $\Delta m \leq 20$ GeV/c^2 :
  For high gluino masses, the energy deposited by the neutral R-hadrons is quite small. In this respect, the gluino is not so different from a neutralino, and the $\widetilde{q}_1 \rightarrow q\widetilde{g}$ events resemble $\widetilde{q}_1 \rightarrow q\widetilde{\chi}_1^0$ events.
- $\Delta m > 20$ GeV/c^2 :
  In this case, the gluino deposits more energy.

The neural networks were trained to isolate the $q\bar{q}R^{\circ}R^{\circ}$ signal in both Δm windows. They were trained separately on stop signals or sbottom signals. The neural network structure was the same for the stop and the sbottom searches. It consisted of 10 input nodes, 10 hidden nodes and 3 output nodes.

For $\Delta m \leq 20$ GeV/c^2, the 10 input variables were: the ratio between the transverse missing momentum and the visible energy, the transverse energy, the visible mass, the softness defined as $M_{jet1}/E_{jet1} + M_{jet2}/E_{jet2}$, the acollinearity, the quadratic sum of transverse momenta of the jets $\sqrt{(P_t^{jet1})^2 + (P_t^{jet2})^2}$, the acoplanarity, the sum of the first and third Fox-Wolfram moments, the polar angle of the missing momentum and finally the combined b-tagging probability [22].

For $\Delta m > 20$ GeV/c^2, the 10 input variables were: the charged energy, the transverse charged energy, the visible mass, the thrust, the effective centre-of-mass energy [23], the acollinearity, the acoplanarity, the sum of the first and third Fox-Wolfram moments, the sum of the second and fourth Fox-Wolfram moments, and finally the combined b-tagging probability.

The neural networks were trained to discriminate the signal from the combined two-fermion and four-fermion backgrounds, and from the $\gamma\gamma$ interactions leading to hadronic

final states. The first output node was trained to identify both $Z^0 \to q\bar{q}$ and four-fermion events. The second node identified the $\gamma\gamma$ interactions leading to hadronic final states. And the third node was trained to select the signal. The three output nodes were useful in the training of the network, but the selection was made according to the output of the signal node only. Figure 15 shows the number of events as a function of the signal efficiency for the two mass analysis windows of the stop and the sbottom analysis. The number of real events was in agreement with the Standard Model predictions over the full range of the neural network outputs. The optimisations of the final cuts were performed by minimising the expected confidence level of the signal hypothesis [24].

Tables 8 and 9 contain the numbers of events selected in the stop and sbottom analyses. Combining all data from 189 to 208 GeV, 32 and 11 events were selected in the stop analysis for $\Delta m > 20$ GeV/c^2 and $\Delta m \leq 20$ GeV/c^2, while the expected number of events were 30.1 and 11.1. In the sbottom analysis, no candidates were observed for $\Delta m > 20$ GeV/c^2 and five were selected for $\Delta m \leq 20$ GeV/c^2. The expected number of events were 3.0 and 5.3. Figure 16 shows the signal detection efficiencies for the stop and for the sbottom ($m_{\tilde{q}_1} = 90$ GeV/c^2). They are very low when the gluino mass is close to zero.

8 Results

No excess of events was observed in any analysis performed at LEP1 or at LEP2 in the stable gluino scenario. Results were therefore combined to obtain excluded regions at 95% confidence level in the parameter space. The limits were computed using the likelihood ratio method described in [24]. For different values of the parameter P describing the probability that the gluino hadronizes to a charged R-hadron, the relative cross-sections for the different channels were given by:

$$\begin{cases} \sigma(\mathrm{R}^{\pm}\mathrm{R}^{\pm}) &= P^2\sigma \\ \sigma(\mathrm{R}^{\pm}\mathrm{R}^{\circ}) &= 2P(1-P)\sigma \\ \sigma(\mathrm{R}^{\circ}\mathrm{R}^{\circ}) &= (1-P)^2\sigma \end{cases}$$

where σ was either the $e^+e^- \to q\bar{q}\tilde{g}\tilde{g}$ cross section at LEP1, the $\tilde{t}_1\bar{\tilde{t}}_1$ or the $\tilde{b}_1\bar{\tilde{b}}_1$ cross-section at LEP2.

For the LEP1 analysis, results were interpreted in terms of excluded gluino masses for different P. Figure 17 shows the excluded region at 95% confidence level. From this figure, a stable gluino with mass between 2 and 18 GeV/c^2 is excluded regardless of the charge of the R-hadrons. The minimum upper limit, 18 GeV/c^2, is obtained for intermediate values of P (between 0.2 and 0.45), while an upper limit of 23 GeV/c^2 is obtained for P=1.

For the LEP2 analysis, excluded regions in the planes ($m_{\tilde{t}_1}$,$m_{\tilde{g}}$) and ($m_{\tilde{b}_1}$,$m_{\tilde{g}}$) were derived for five different values of P: 0., 0.25, 0.5, 0.75 and 1. Moreover, the stop and sbottom cross-sections were calculated for two cases. In the first case, the squark mixing angle was set to zero which corresponds to the maximal cross-sections. In the second case, the mixing angle was equal to 56° for the stop and to 68° for the sbottom, which gives the minimal cross-sections. Squark masses below 50 GeV/c^2 were not taken into account in these analyses. Figures 18 and 19 show the excluded regions thus obtained. In the case of minimal cross-sections, a hole appears in the sbottom exclusion histograms around (60 GeV/c^2, 50GeV/c^2) in the plane ($m_{\tilde{b}_1}$,$m_{\tilde{g}}$) for intermediate values of P. It can be explained by different effects:

- In the analyses searching for charged R-hadrons, the signal detection efficiencies are small in this region of the ($m_{\tilde{q}_1}$,$m_{\tilde{g}}$) plane, because the dE/dx distribution of the charged R-hadrons as a function of the momentum crosses the band corresponding to Standard Model particles (cf Figure 6).
- When the $Z^0-\widetilde{q}_1-\bar{\widetilde{q}}_1$ coupling is suppressed, the squark pair production cross-section is much more reduced for the sbottom than for the stop.
- The visible energy of $q\bar{q}R^\circ R^\circ$ events becomes small for low values of ΔM. At $\Delta M = 5$ GeV/c^2, this has no effect on the stop exclusion results, because of the c-quark which is lighter than the b-quark.

Lower limits on the stop and sbottom masses are given in table 10 for $\Delta m \geq 10$ GeV/c^2 and for a gluino mass greater than 2 GeV/c^2 for different values of P.

9 Conclusion

The analysis of the LEP1 data collected in 1994 excludes at 95% confidence level a stable gluino with mass between 2 and 18 GeV/c^2. These limits are valid for any charge of the produced R-hadrons.

Stop and sbottom squarks have been searched for in the 609 pb^{-1} collected by DELPHI at centre-of-mass energies ranging from 189 to 208 GeV. In the stable gluino scenario, the dominant decays are $\widetilde{t}_1 \rightarrow c\widetilde{g}$ and $\widetilde{b}_1 \rightarrow b\widetilde{g}$. No deviation from Standard Model predictions was observed. The observed limits at 95% confidence level are:

- $m_{\tilde{t}_1} > 90$ GeV/c^2, and $m_{\tilde{b}_1} > 96$ GeV/c^2 for purely left squarks.
- $m_{\tilde{t}_1} > 87$ GeV/c^2, and $m_{\tilde{b}_1} > 82$ GeV/c^2 independent of the mixing angle.

Acknowledgements

We are greatly indebted to our technical collaborators, to the members of the CERN-SL Division for the excellent performance of the LEP collider, and to the funding agencies for their support in building and operating the DELPHI detector.
We acknowledge in particular the support of
Austrian Federal Ministry of Education, Science and Culture, GZ 616.364/2-III/2a/98,
FNRS–FWO, Flanders Institute to encourage scientific and technological research in the industry (IWT), Belgium,
FINEP, CNPq, CAPES, FUJB and FAPERJ, Brazil,
Czech Ministry of Industry and Trade, GA CR 202/99/1362,
Commission of the European Communities (DG XII),
Direction des Sciences de la Matière, CEA, France,
Bundesministerium für Bildung, Wissenschaft, Forschung und Technologie, Germany,
General Secretariat for Research and Technology, Greece,
National Science Foundation (NWO) and Foundation for Research on Matter (FOM), The Netherlands,
Norwegian Research Council,
State Committee for Scientific Research, Poland, SPUB-M/CERN/PO3/DZ296/2000, SPUB-M/CERN/PO3/DZ297/2000, 2P03B 104 19 and 2P03B 69 23(2002-2004)
JNICT–Junta Nacional de Investigação Científica e Tecnológica, Portugal,
Vedecka grantova agentura MS SR, Slovakia, Nr. 95/5195/134,
Ministry of Science and Technology of the Republic of Slovenia,

CICYT, Spain, AEN99-0950 and AEN99-0761,
The Swedish Natural Science Research Council,
Particle Physics and Astronomy Research Council, UK,
Department of Energy, USA, DE-FG02-01ER41155.

References

[1] H. Baer, K. Cheung, J.F. Gunion, Phys. Rev. **D59** (1999) 075002.
[2] A. Mafi, S. Raby, Phys. Rev. **D62** (2000) 35003.
A. Mafi, S. Raby, Phys. Rev. **D63** (2001) 55010.
[3] CDF Collaboration, F. Abe *et al.*, Phys. Rev. Lett. **79** (357) 1997.
D0 Collaboration, S., Abachi *et al.*, Phys. Rev. Lett. **83** (4937) 1999.
[4] G.R. Farrar, Nucl. Phys. Proc. Suppl. **62** (1998) 485.
[5] ALEPH Collaboration, R. Barate *et al.*, Z. Phys. **C76** (1997) 1.
DELPHI Collaboration, P. Abreu *et al.*, Phys. Lett. **B414** (1997) 401.
L3 Collaboration, M. Acciarri *et al.*, Phys. Lett. **B489** (2000) 65.
OPAL Collaboration, G. Abbiendi *et al.*, E. Phys. J. **C20** (2001) 601.
[6] K. Hikasa, M.Kobayashi, Phys. Rev. **D36** (1987) 724.
[7] DELPHI Collaboration, P. Aarnio *et al.*, Nucl. Instr. and Meth. **A303** (1991) 233.
[8] DELPHI Collaboration, P. Abreu *et al.*, Nucl. Instr. and Meth. **A378** (1996) 57.
[9] T. Sjöstrand, Comp. Phys. Comm. **82** (1994) 74.
[10] DELPHI Collaboration, P. Abreu *et al.*, Z. Phys. **C73** (1996) 11.
[11] F.A. Berends, R. Pittau, R. Kleiss, Comp. Phys. Comm. **85** (1995) 437.
[12] J. Fujimoto *et al.*, Comp. Phys. Comm. **100** (1997) 128.
[13] S. Jadach, B.F.L. Ward, Z. Was, Comp. Phys. Comm. **124** (2000) 23.
[14] S. Jadach, W. Placzek, B.F.L. Ward, Phys. Lett. **B390** (1997) 298.
[15] C. Friberg, T. Sjöstrand, JHEP **9** (2000) 10.
[16] F.A. Berends, P.H. Daverveldt, R. Kleiss, Comp. Phys. Comm. **40** (1986) 271.
[17] S. Katsanevas, P. Morawitz, Comp. Phys. Comm. **112** (1998) 227.
[18] M. Drees, J.P. Eboli, E. Phys. J. **C10** (1999) 337.
[19] C. Peterson, D. Schatter, I. Scmitt, P.M. Zerwas, Phys. Rev. **D27** (1983) 105.
[20] DELPHI Collaboration, P. Aarnio *et al.*, Nucl. Instr. and Meth. **303** (1991) 233.
[21] S. Catani *et al.*, Phys. Lett. **B269** (91) 432.
[22] G. Borisov, Nucl. Instr. and Meth. **A417** (1998) 384.
[23] P. Abreu *et al.*, Nucl. Instr. and Meth. **A427** (1999) 487.
[24] A. Read, CERN Report 2000-05, p. 81 (2000).

	Data	$Z^0 \to q\bar{q}$ background
anomalous dE/dx	99322	97170 ± 200
Y_{23}	24566	25794 ± 104
1 $R^{\pm}$ candidate	421	464 ± 14
low dE/dx ($m_{\tilde{g}} < 14$)	5	4.2 ± 1.3
high dE/dx ($m_{\tilde{g}} \geq 14$)	12	13.5 ± 2.4

Table 2: Number of events selected after each cut of the charged R-hadron analysis at LEP1.

	Data	$Z^0 \to q\bar{q}$ background
Acolinearity	41231	34853 ± 120
N_{TPC}	38977	33807 ± 120
$\%E_{VD-ID}$	36877	32419 ± 120
E_{40}/E_{vis}	19309	15311 ± 80
E_{20}/E_{vis}	16664	13480 ± 75
E_t	16317	13453 ± 75
M_{vis}	5932	6353 ± 52
$\lvert\cos\theta_{thrust}\rvert$	5384	5725 ± 49
$\lvert\cos\theta_{Pmis}\rvert$	2527	2294 ± 31
Y_{23}	214	194 ± 9
$N_{char.}$	183	161 ± 8
Acoplanarity	134	115 ± 7
Thrust	105	81.7 ± 5.9
Acol. vs $M_{jet1}/E_{jet1} + M_{jet2}/E_{jet2}$	12	10.6 ± 2.1

Table 3: Number of events selected after each cut of the $q\bar{q}R^{\circ}R^{\circ}$ analysis at LEP1.

Cuts	Data	Simulation	4-fermions	2-fermions	$\gamma\gamma$
N_{TPC}	175436	164146 ± 105	12418 ± 13	50391 ± 24	101338 ± 102
$E_{STIC}/E_{vis.}$	145810	141362 ± 95	12062 ± 13	48170 ± 24	81131 ± 91
θ_{thrust}	54838	54933 ± 45	9739 ± 10	31510 ± 23	13685 ± 38
P_{TPC}	48475	48846 ± 43	9141 ± 10	27580 ± 23	12126 ± 35
$N_{cha.}$	45816	46227 ± 37	9040 ± 9	26969 ± 16	10219 ± 32
$E^{max.}_{neu.}$	41880	42113 ± 37	8802 ± 9	23108 ± 16	10203 ± 32
1 $R^{\pm}$ candidate	2187	2279.1 ± 6.3	1746.8 ± 4.6	470.3 ± 3.4	62.6 ± 2.6
2 $R^{\pm}$ candidates	74	79.2 ± 0.8	75.2 ± 0.7	3.4 ± 0.3	0.5 ± 0.2

Table 4: Number of events after each cut of the LEP2 preselection. 189 to 208 GeV data are added.

	$m_{\tilde{g}} \leq 30$ GeV/c^2		30 GeV/c^2 $< m_{\tilde{g}} <$ 60 GeV/c^2		$m_{\tilde{g}} \geq 60$ GeV/c^2	
$\sqrt{s}$	Data	Simulation	Data	Simulation	Data	Simulation
188.7	0	0.029±0.016	0	0.001±0.001	0	0.003±0.003
191.6	0	0.005±0.004	0	0.001±0.001	0	0.001±0.001
195.6	0	0.025±0.020	0	0.001±0.001	0	0.001±0.001
199.6	0	0.007±0.007	0	0.001±0.001	0	0.001±0.001
201.7	0	0.011±0.007	0	0.001±0.001	0	0.001±0.001
204.8	0	0.009±0.009	0	0.001±0.001	0	0.001±0.001
206.7	0	0.012±0.009	0	0.001±0.001	0	0.001±0.001
208.1	0	0.000±0.000	0	0.001±0.001	0	0.001±0.001
206.5(*)	0	0.017±0.013	0	0.001±0.001	0	0.001±0.001
total	0	0.115±0.033	0	0.009±0.003	0	0.011±0.004

Table 5: Number of events selected by the $q\bar{q}R^{\pm}R^{\pm}$ analysis at LEP2. (*) indicates 2000 data taken without sector 6 working.

	$m_{\tilde{g}} \leq 30$ GeV/c^2		30 GeV/c^2 $< m_{\tilde{g}} <$ 60 GeV/c^2		$m_{\tilde{g}} \geq 60$ GeV/c^2	
$\sqrt{s}$	Data	Simulation	Data	Simulation	Data	Simulation
188.7	0	0.577±0.101	0	2.514±0.264	0	1.937±0.243
191.6	0	0.030±0.011	1	0.454±0.132	1	0.425±0.131
195.6	2	0.135±0.042	2	0.783±0.097	0	0.648±0.088
199.6	0	0.266±0.071	1	1.333±0.158	1	1.068±0.141
201.7	0	0.097±0.025	2	0.489±0.056	2	0.392±0.050
204.8	1	0.208±0.051	1	0.961±0.106	0	0.753±0.093
206.6	0	0.187±0.040	1	0.848±0.089	1	0.661±0.079
208.1	0	0.011±0.005	0	0.095±0.014	0	0.085±0.013
206.5(*)	0	0.083±0.025	1	0.679±0.074	1	0.596±0.070
total	3	1.59±0.15	9	8.16±0.39	6	6.57±0.36

Table 6: Number of events selected by the $q\bar{q}R^{\pm}R^{\circ}$ analysis at LEP2. (*) indicates 2000 data taken without sector 6 working.

Cuts	Data	simulation	4-fermions	2-fermions	$\gamma\gamma$
$P_t^{mis.}$	26423	26938 ± 20	8117 ± 8	18012 ± 15	809 ± 9
$\theta_{P_{mis.}}$	16379	16821 ± 15	7191 ± 6	9088 ± 12	542 ± 8
$E_{40^0}/E_{vis.}$	14694	15231 ± 14	6395 ± 6	8471 ± 12	364 ± 6
Hermeticity	14422	14651 ± 14	6150 ± 6	8140 ± 12	361 ± 6

Table 7: $q\bar{q}R^{\circ}R^{\circ}$ analysis at LEP2: number of events after each selection cut. Data with $\sqrt{s}$ in the range 189 GeV-208 GeV are included.

	$\Delta M > 20$ GeV/c^2		$\Delta M \leq 20$ GeV/c^2	
$\sqrt{s}$	Data	Simulation	Data	Simulation
188.7	4	6.634±0.741	6	3.685±1.158
191.6	4	1.054±0.115	0	0.482±0.097
195.6	5	3.532±0.236	3	1.408±0.256
199.6	7	4.324±0.270	0	1.617±0.280
201.7	1	2.055±0.140	0	0.836±0.138
204.8	4	4.432±0.302	0	1.197±0.268
206.6	5	4.287±0.290	2	1.227±0.272
208.1	0	0.418±0.031	0	0.117±0.026
206.5(*)	2	3.411±0.203	0	0.556±0.072
total	32	30.2±1.0	11	11.1±1.3

Table 8: Number of events selected by the stop $q\bar{q}R^{\circ}R^{\circ}$ analysis. (*) indicates 2000 data taken without sector 6 working.

	$\Delta M > 20$ GeV/c^2		$\Delta M \leq 20$ GeV/c^2	
$\sqrt{s}$	Data	Simulation	Data	Simulation
188.7	0	1.038±0.657	3	2.475±1.139
191.6	0	0.085±0.026	0	0.180±0.058
195.6	0	0.314±0.088	1	0.571±0.178
199.6	0	0.295±0.094	0	0.663±0.195
201.7	0	0.225±0.049	1	0.319±0.096
204.8	0	0.295±0.040	0	0.428±0.174
206.6	0	0.312±0.05	0	0.379±0.175
208.1	0	0.022±0.005	0	0.037±0.017
206.5(*)	0	0.417±0.054	0	0.281±0.160
total	0	3.0±0.7	5	5.3±1.2

Table 9: Number of events selected by the sbottom $q\bar{q}R^{\circ}R^{\circ}$ analysis. (*) indicates 2000 data taken without sector 6 working.

	Stop		Sbottom	
P	$\theta_{\tilde{t}} = 0°$	$\theta_{\tilde{t}} = 56°$	$\theta_{\tilde{b}} = 0°$	$\theta_{\tilde{b}} = 68°$
0.00	92	87	98	86
0.25	90	87	96	82
0.50	92	89	94	82
0.75	94	92	94	84
1.00	95	94	95	87

Table 10: Upper limits on the stop and sbottom masses as a function of the probability P that the gluino hadronizes to charged R-hadrons. Limits are set for $\Delta m \geq 10$ GeV/c^2 and for a gluino mass greater than 2 GeV/c^2. Mixing angles equal to zero corresponds to purely left-handed squarks, while $\theta_{\tilde{t}} = 56°$ and $\theta_{\tilde{b}} = 68°$ corresponds to minimal cross-section case.

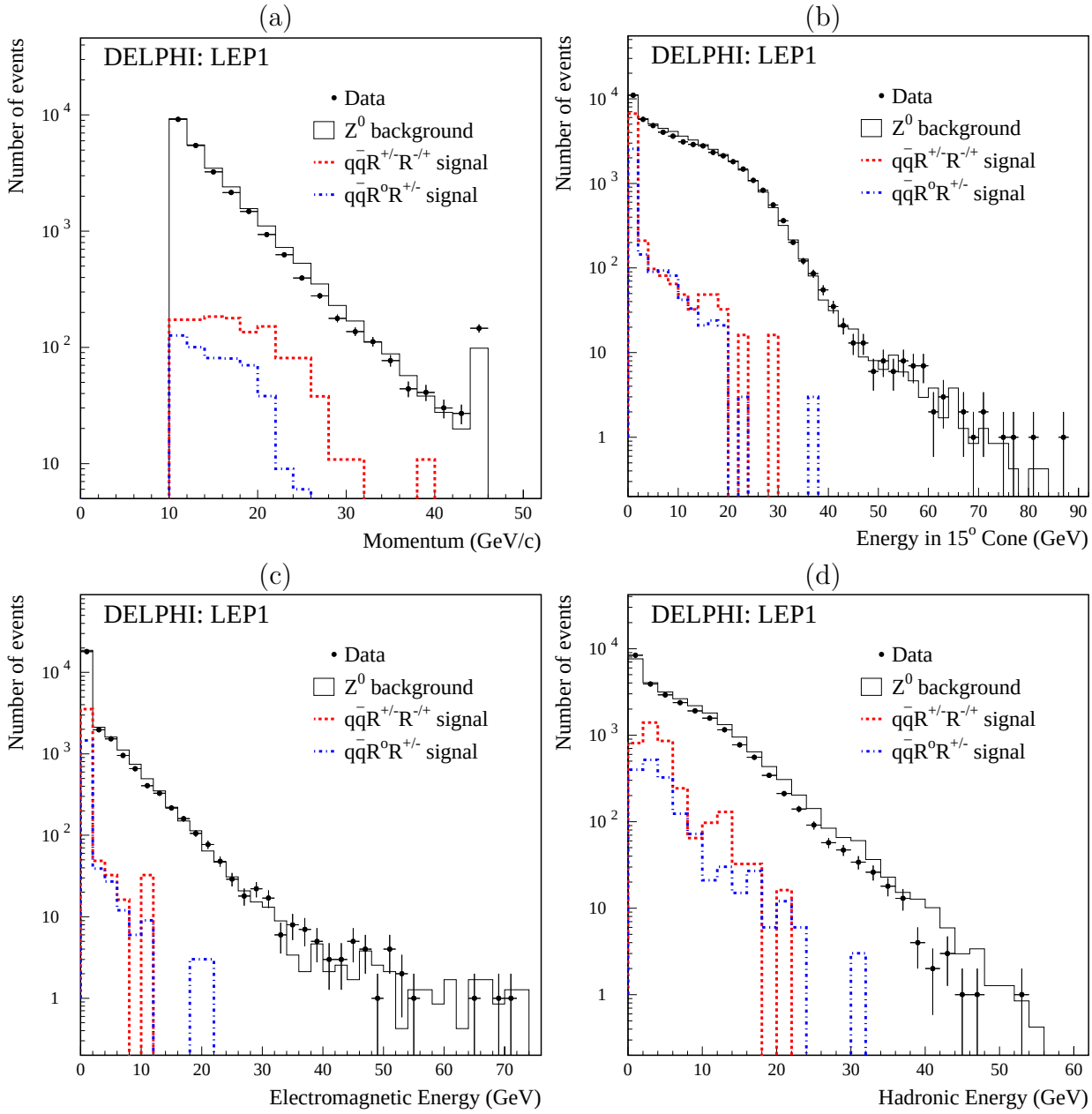

Figure 5: Comparison between data and simulation in the search for charged R-hadrons at LEP1. The plots show characteristic distributions before the selection of the charged R-hadron candidates: (a) the momentum, (b) the total energy in a 15° degree cone around the particle, (c) its electromagnetic and (d) hadronic energy. Dotted lines show the $q\bar{q}R^{\pm}R^{\pm}$ and $q\bar{q}R^{\pm}R^{\circ}$ signal distributions with arbitrary normalization when all simulated samples are added together.

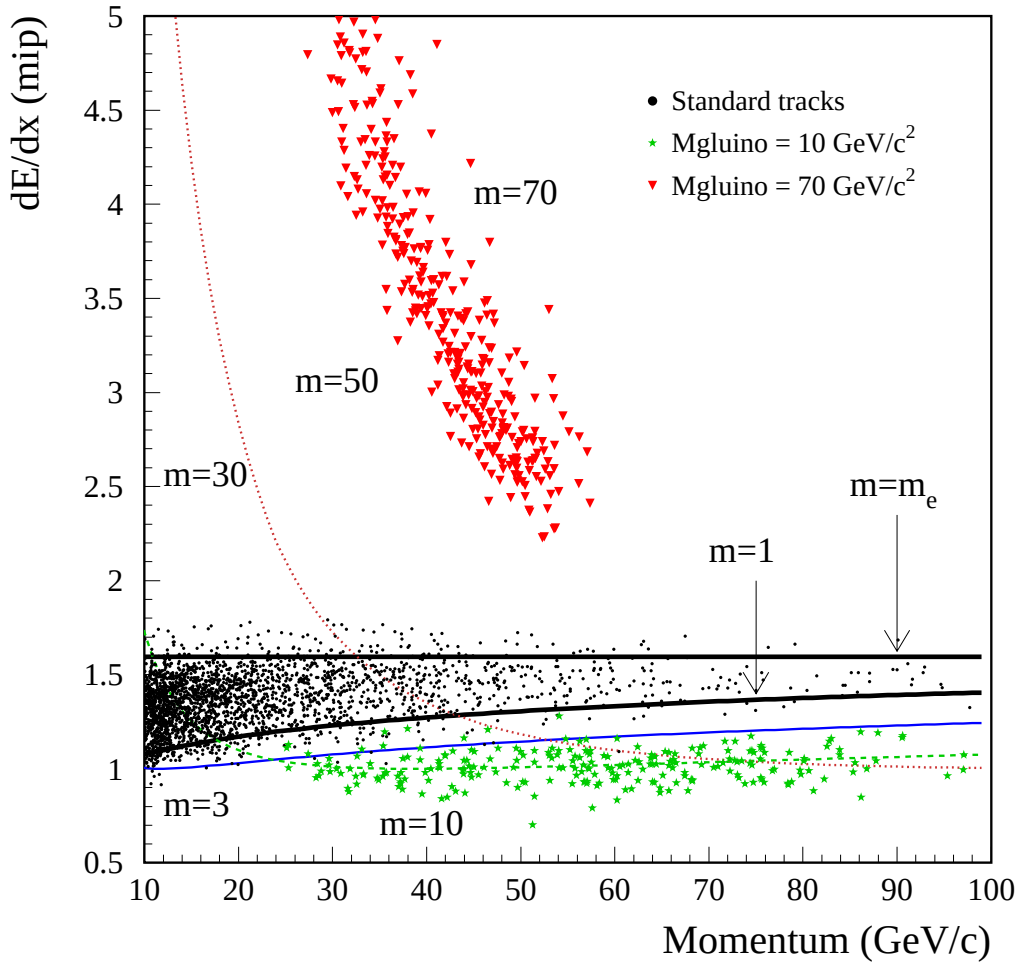

Figure 6: The lines show the theoritical ionization energy loss as a function of the momentum of the particle for different mass cases (GeV/c^2). The black points are reconstructed tracks coming from $Z^0 \rightarrow q\bar{q}$ events generated at $\sqrt{s}$ =200 GeV, while the stars and the triangles correspond to $R^{\pm}$ tracks with mass of 10 and 70 GeV/c^{2}respectively. The dE/dx is expressed in units of energy loss for a minimum ionizing particle.

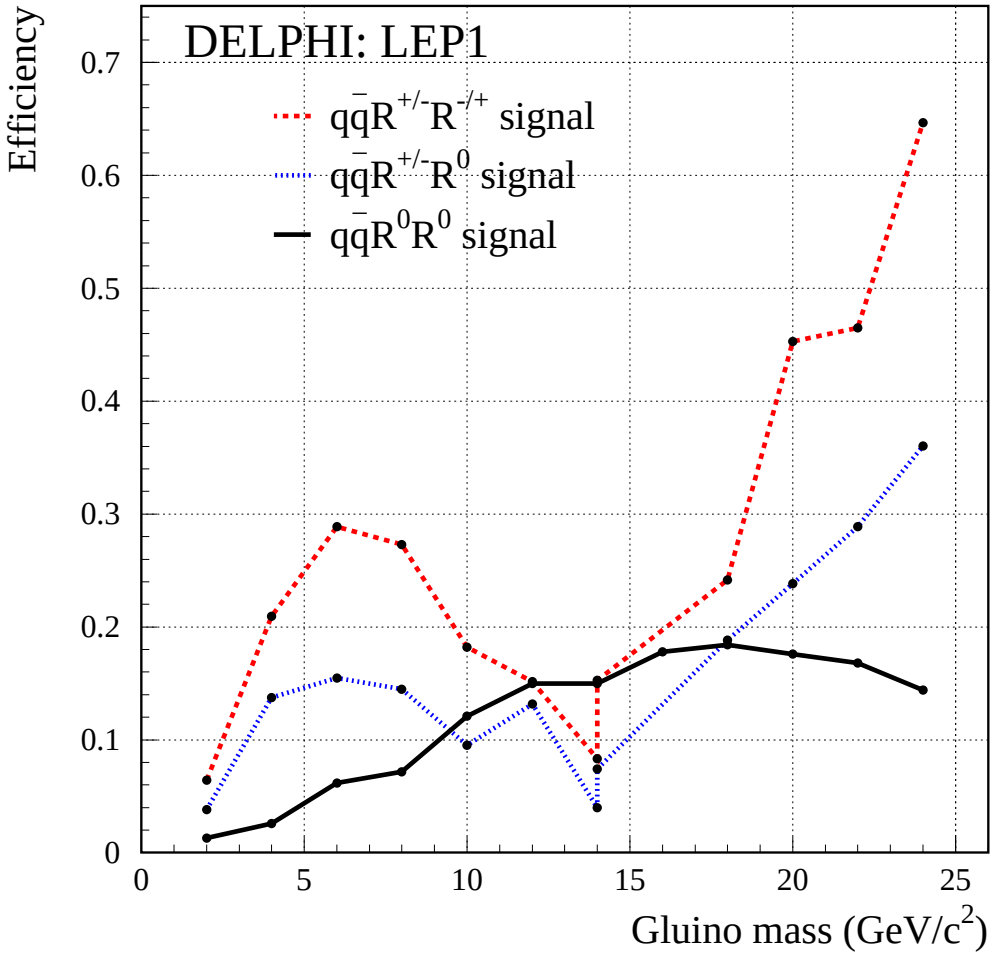

Figure 7: Signal detection efficiencies in the LEP1 data analyses as a function of the gluino mass for the three signal topologies $q\bar{q}R^{\pm}R^{\pm}$, $q\bar{q}R^{\pm}R^{\circ}$ and $q\bar{q}R^{\circ}R^{\circ}$. The search for charged R-hadrons was optimized separately for low gluino masses (< 14 GeV/c^2) and for high gluino masses (≥ 14 GeV/c^2).

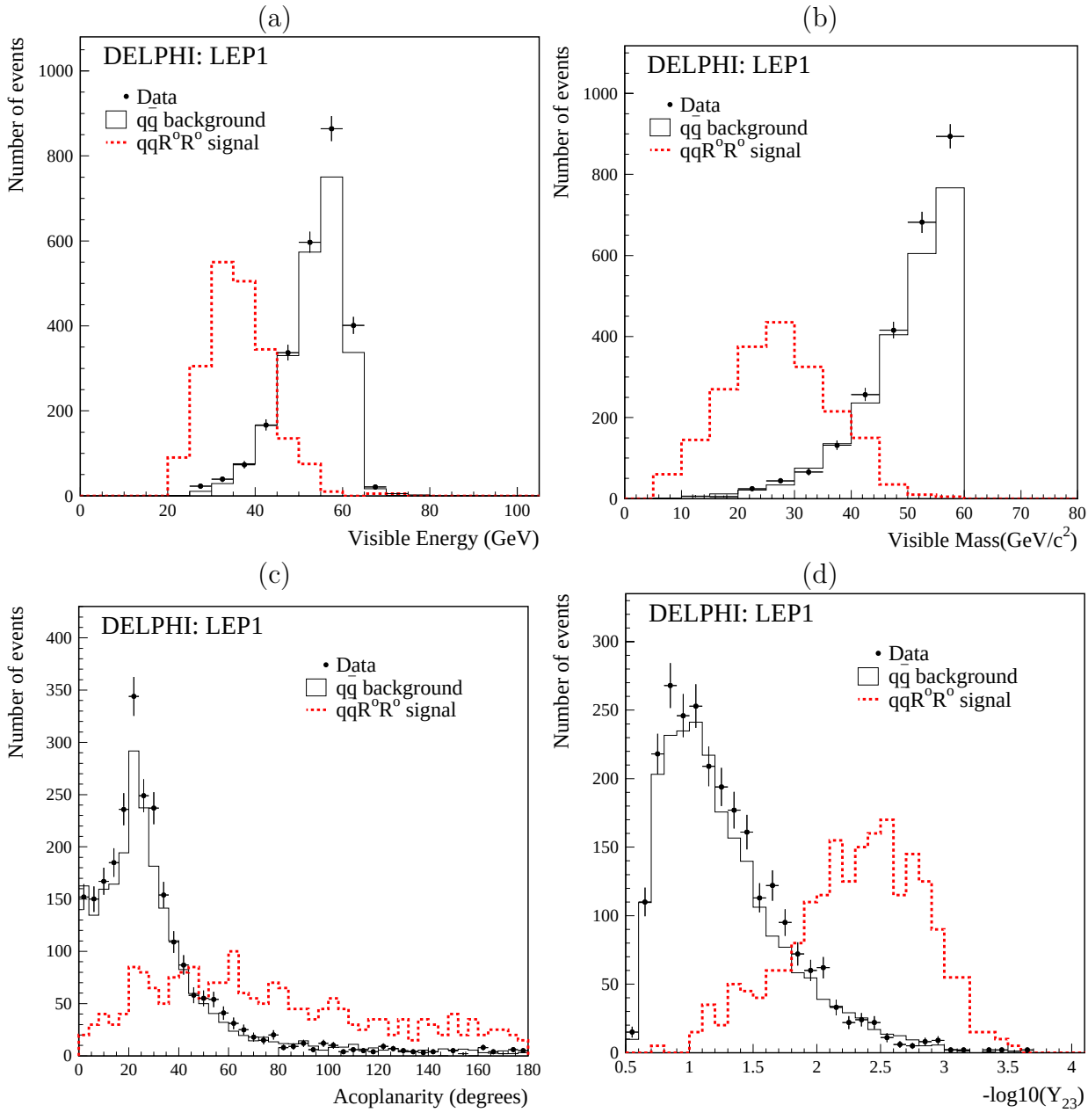

Figure 8: Comparison between data and simulation in the $q\bar{q}R^{\circ}R^{\circ}$ analysis at LEP1. (a) visible energy, (b) visible mass, (c) acoplanarity (d) DURHAM distance Y_{23}. Dotted lines show the $q\bar{q}R^{\circ}R^{\circ}$ signal distributions with arbitrary normalization when all simulated samples are added together.

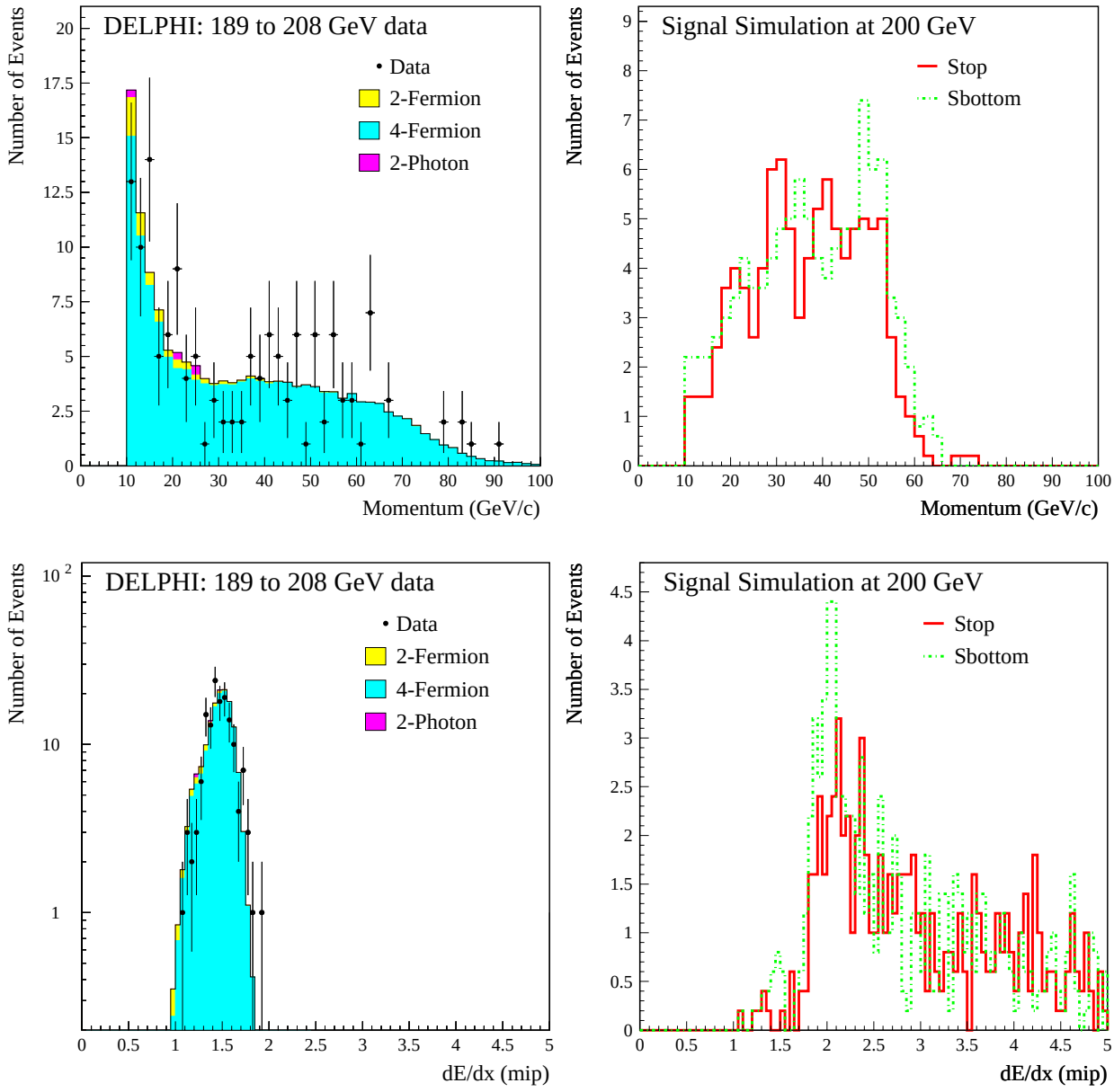

Figure 9: Momentum and dE/dx of the charged R-hadron candidates selected by the $q\bar{q}R^{\pm}R^{\pm}$ analysis at LEP2. Data taken in the centre-of-mass energy range between 189 and 208 GeV were included. Right-hand side histograms show the expected distributions for one possible stop and sbottom signal ($m_{\tilde{q}_1} = 90$ GeV/c^2, $m_{\tilde{g}} = 60$ GeV/c^2) at $\sqrt{s} = 200$ GeV with arbitrary normalization.

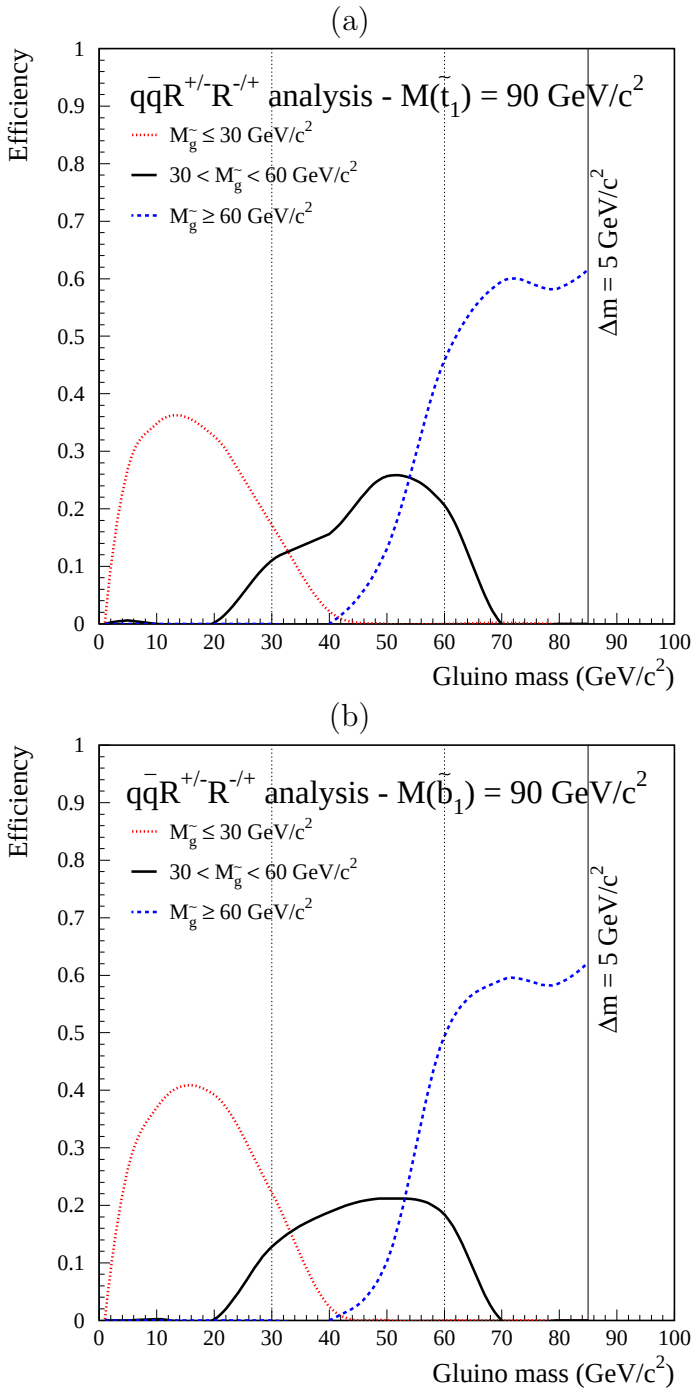

Figure 10: Signal detection efficiencies at $\sqrt{s}$ =200 GeV for the stop (a) and sbottom (b) $q\bar{q}R^{\pm}R^{\pm}$ analysis as a function of the gluino mass ($m_{\tilde{q}_1}$ = 90 GeV/c^2). ΔM is the mass difference between the squark and the gluino. Vertical lines show the limits of the mass analysis window. The last one ends at $\Delta M = 5$ GeV/c^2 which corresponds the last simulated signal points.

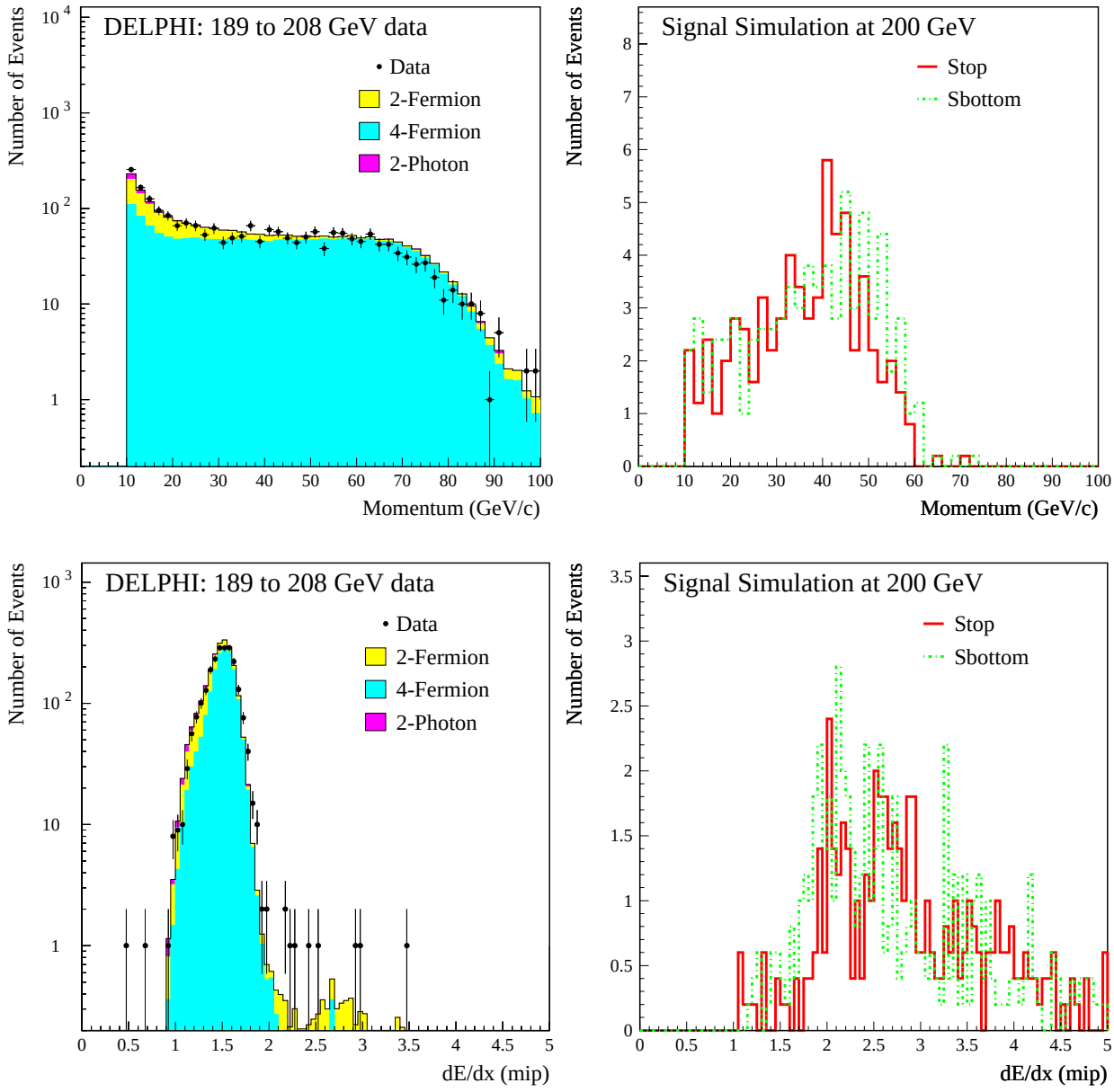

Figure 11: Momentum and dE/dx of the charged R-hadron candidates selected by the $q\bar{q}R^{\pm}R^{\circ}$ analysis at LEP2. Data taken in the centre-of-mass energy range between 189 and 208 GeV were included. Right-hand side histograms show the expected distributions for one possible stop and sbottom signal ($m_{\tilde{q}_1} = 90$ GeV/c^2, $m_{\tilde{g}} = 60$ GeV/c^2) at $\sqrt{s} = 200$ GeV with arbitrary normalization.

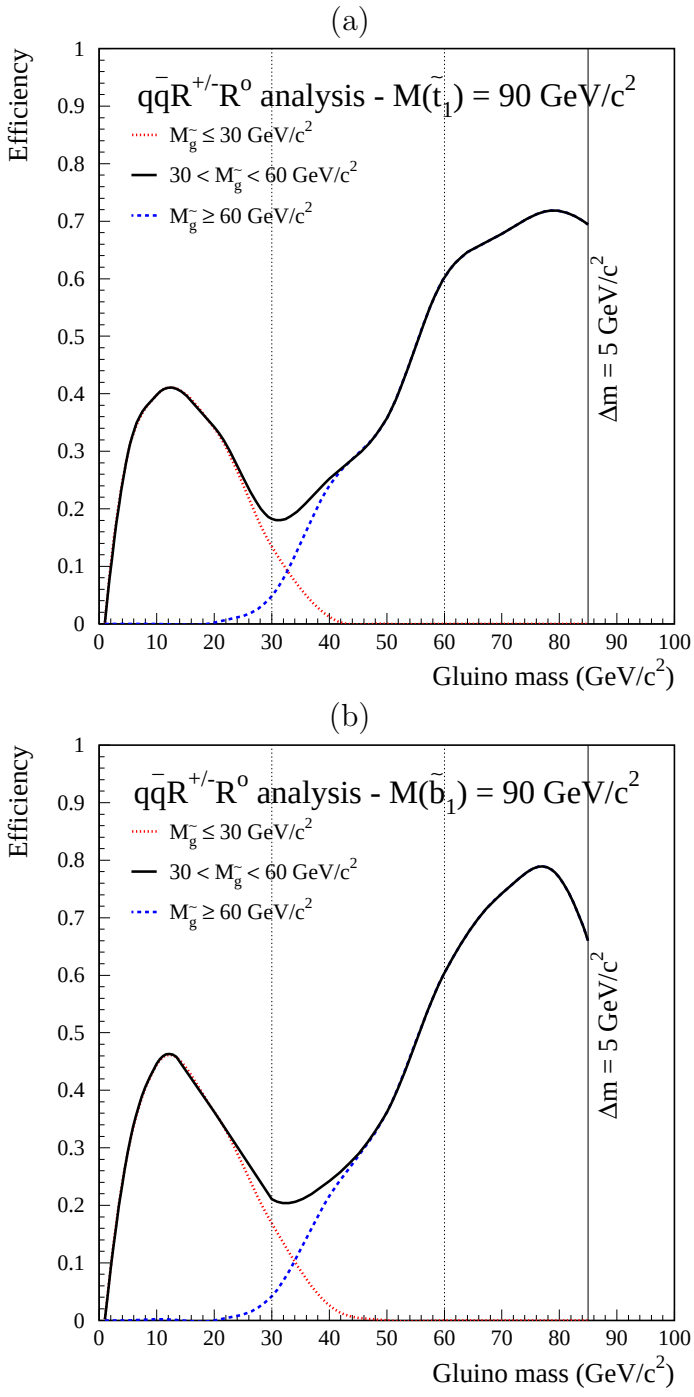

Figure 12: Signal detection efficiencies at $\sqrt{s}$ =200 GeV for the stop (a) and sbottom (b) $q\bar{q}R^{\pm}R^{\circ}$ analysis as a function of the gluino mass ($m_{\tilde{q}_1}$ = 90 GeV/c^2).ΔM is the mass difference between the squark and the gluino. Vertical lines show the limits of the mass analysis window. The last one ends at $\Delta M = 5$ GeV/c^2 which corresponds the last simulated signal points.

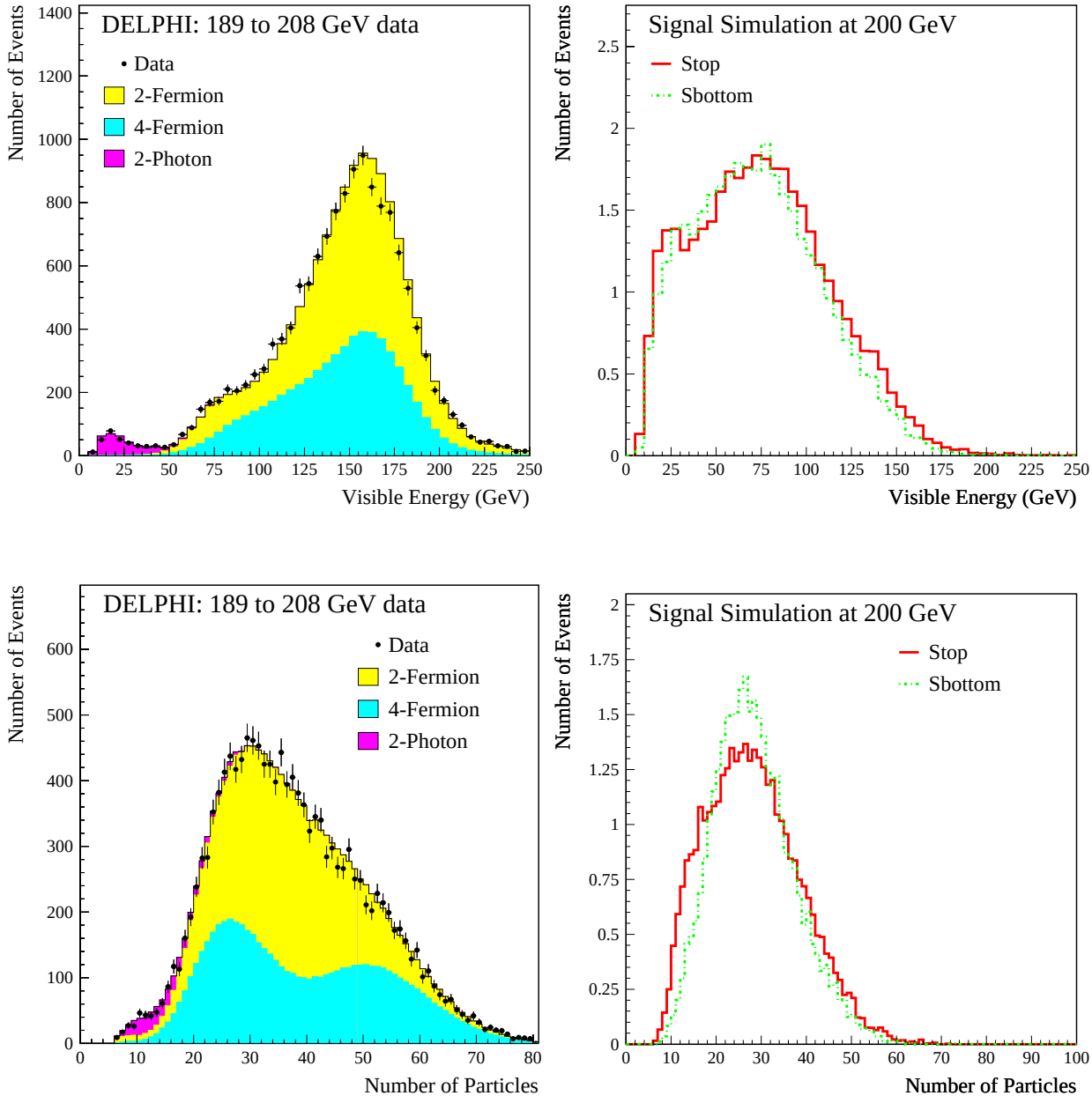

Figure 13: Data-simulation comparison at the preselection level of the LEP2 $q\bar{q}R^{\circ}R^{\circ}$ analysis. Data taken in the centre-of-mass energy range between 189 and 208 GeV were included. Right-hand side histograms show the expected distributions with arbitrary normalization for the stop and the sbottom signal at 200 GeV when all simulated samples are added together.

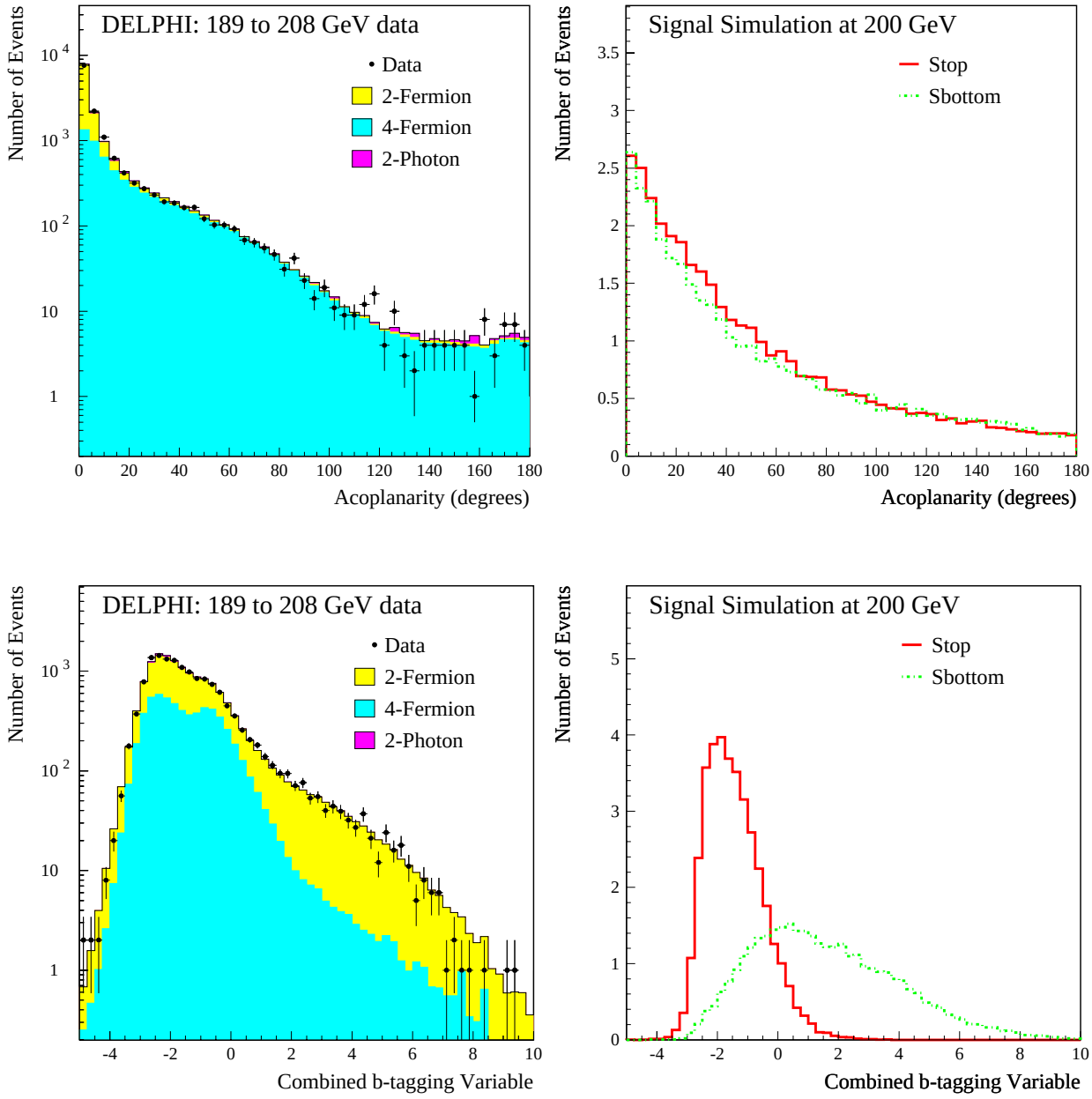

Figure 14: Data-simulation comparison at the preselection level of the LEP2 $q\bar{q}R^{\circ}R^{\circ}$ analysis. Data taken in the centre-of-mass energy range between 189 and 208 GeV were included. Right-hand side histograms show the expected distributions with arbitrary normalization for the stop and the sbottom signal at 200 GeV when all simulated samples are added together.

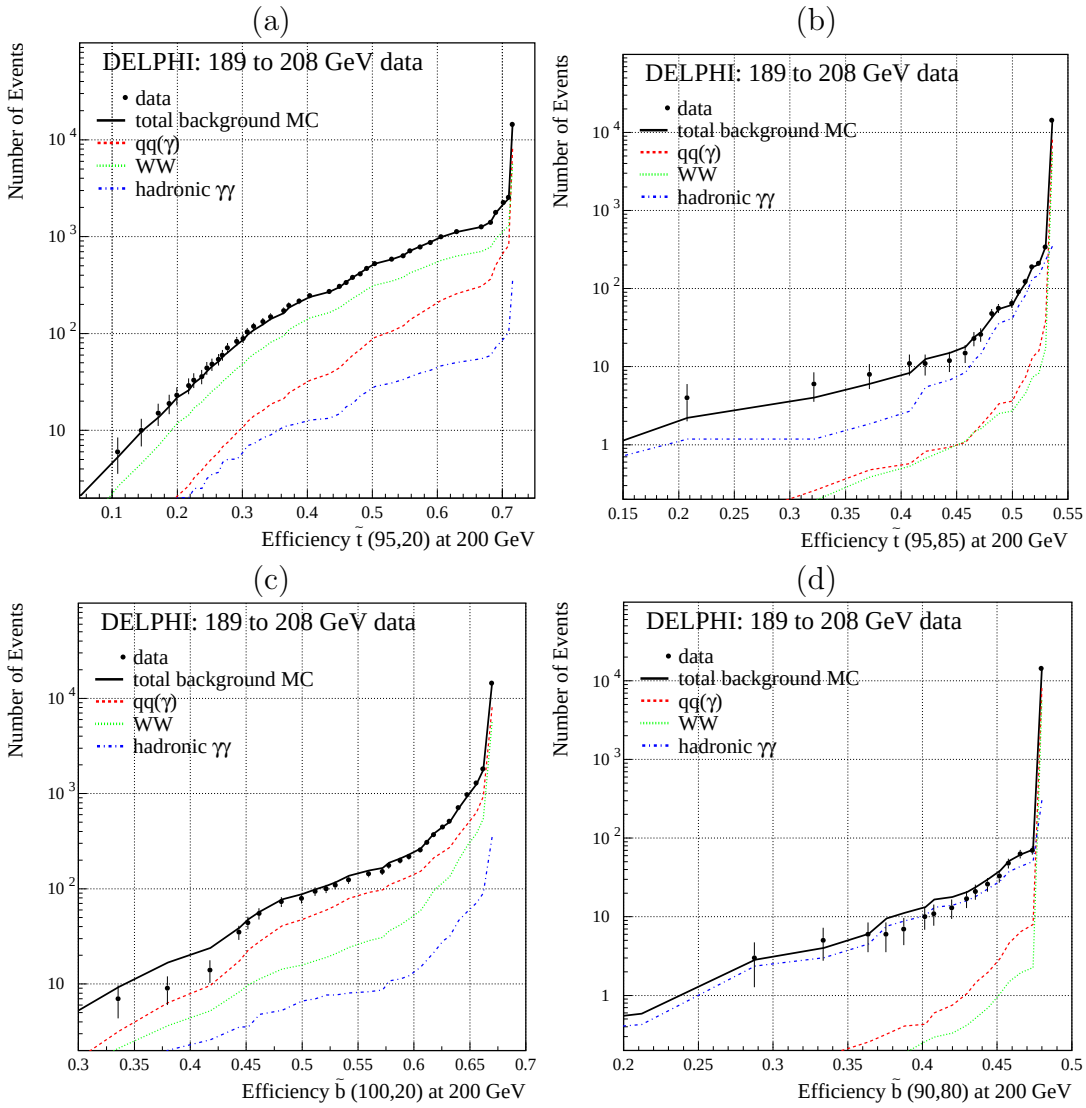

Figure 15: Numbers of events as a function of the signal efficiencies for the stop and sbottom analysis. Data taken in the centre-of-mass energy range between 189 and 208 GeV were included. (a) stop analysis for $\Delta m > 20$ GeV/c^2 and (b) for $\Delta m \leq 20$ GeV/c^2, (c) sbottom analysis for $\Delta m > 20$ GeV/c^2 and (b) for $\Delta m \leq 20$ GeV/c^2. The squark and gluino mass values used for the signal detection efficiencies are indicated on the x axis, $(m_{\tilde{\mathrm{q}}},m_{\tilde{\mathrm{g}}})$.

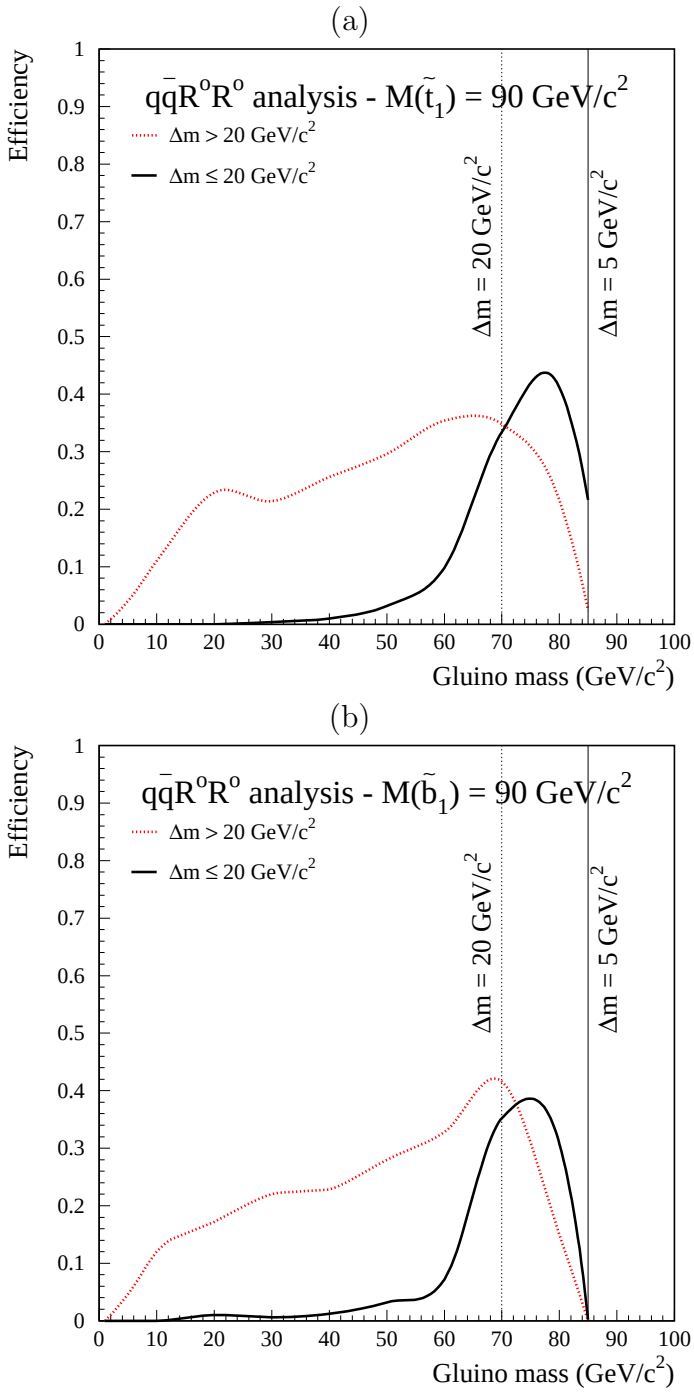

Figure 16: Signal detection efficiencies at $\sqrt{s}$ =200 GeV for the stop (a) and sbottom (b) $q\bar{q}R^{\circ}R^{\circ}$ analysis as a function of the gluino mass ($m_{\tilde{q}_1}$ = 90 GeV/c^2).

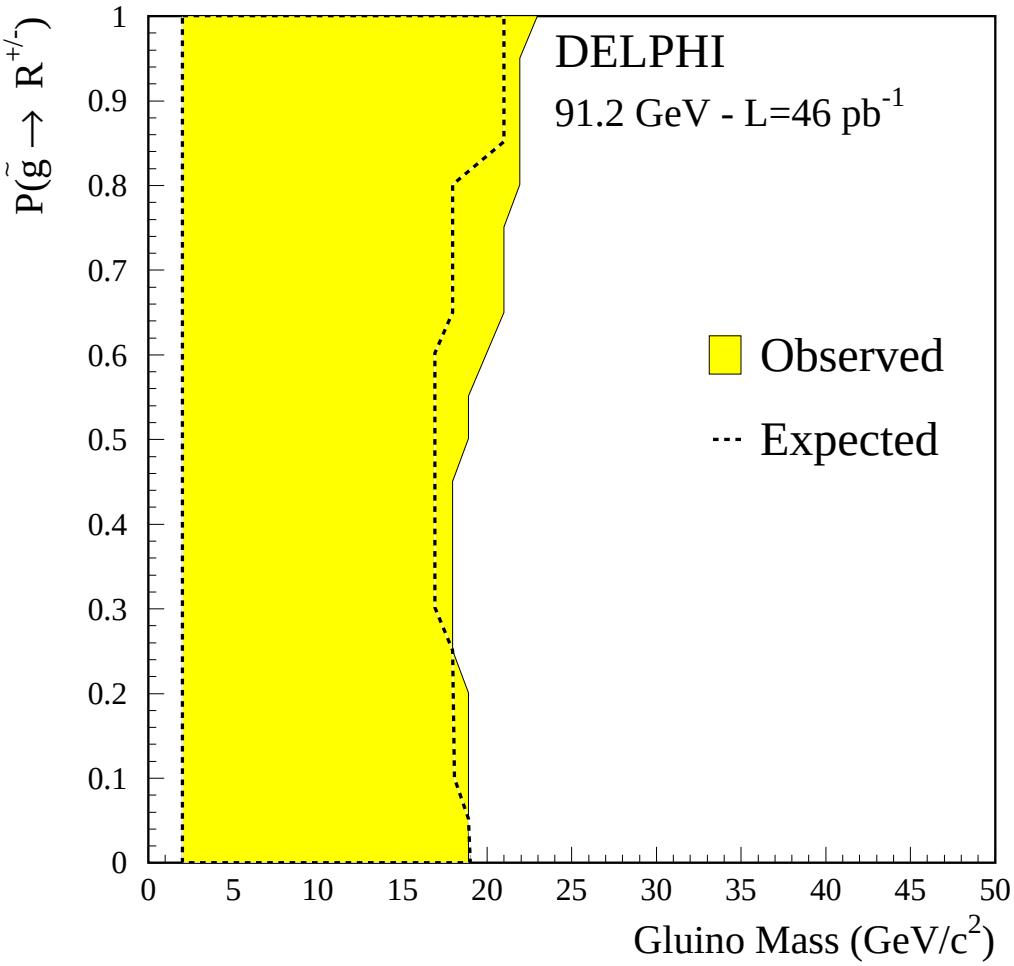

Figure 17: Results of the LEP1 analysis: excluded region at 95% confidence level in the plane ($m_{\tilde{g}}$,P). P is the probability that the gluino hadronizes to a charged R-hadron. The shaded region corresponds to the observed exclusion and the line to the expected one.

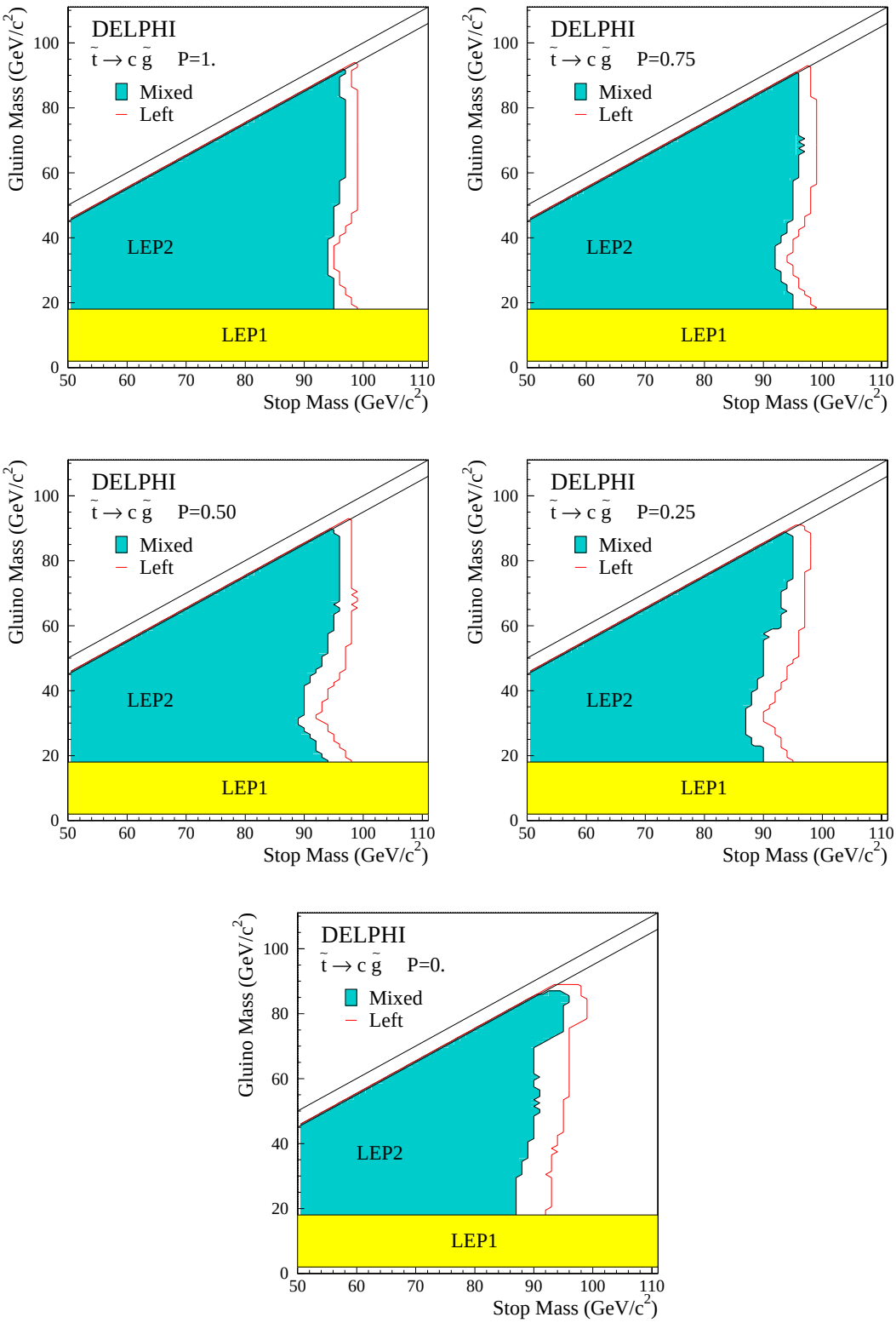

Figure 18: Results of the LEP2+LEP1 stop analysis: excluded region at 95% confidence level in the plane ($m_{\tilde{t}_1}$,$m_{\tilde{g}}$). The line corresponds to the exclusion for purely left stop, and the shaded region to exclusion obtained for the mixing angle giving the minimal cross-section. Excluded regions are given for different values of P, the probability that the gluino hadronizes to charged R-hadron: 0, 0.25, 0.5, 0.75 and 1.

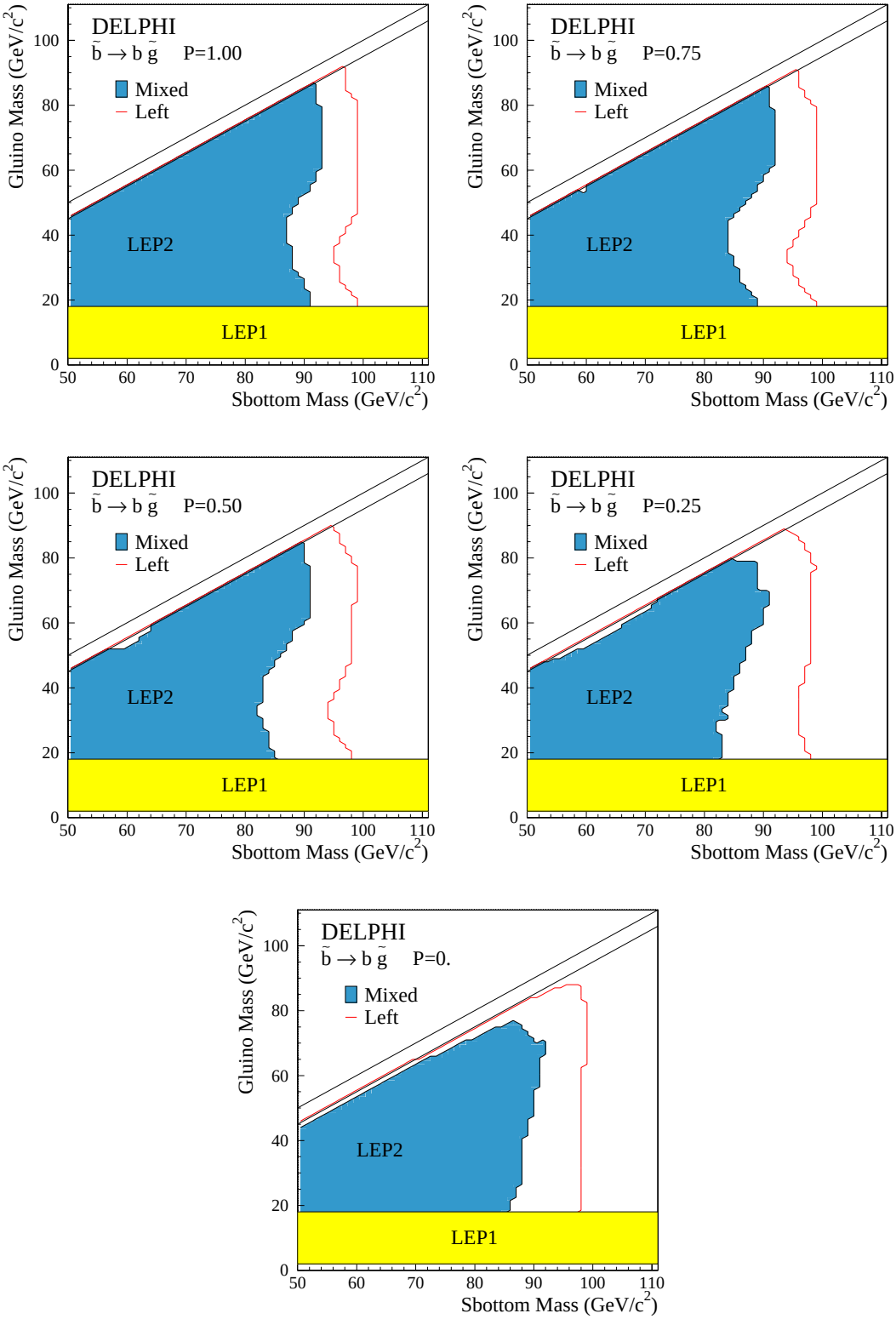

Figure 19: Results of the LEP2+LEP1 sbottom analysis: excluded region at 95% confidence level in the plane ($m_{\tilde{b}_1}$,$m_{\tilde{g}}$). The line corresponds to the exclusion for purely left sbottom, and the shaded region to exclusion obtained for the mixing angle giving the minimal cross-section. Excluded regions are given for different values of P, the probability that the gluino hadronizes to charged R-hadron: 0, 0.25, 0.5, 0.75 and 1.